Bioactive Materials 9 (2022) 475–490

Contents lists available at ScienceDirect

Bioactive Materials

journal homepage: www.sciencedirect.com/journal/bioactive-materials

Silicified collagen scaffold induces semaphorin 3A secretion by sensory nerves to improve *in-situ* bone regeneration

Yu-Xuan Ma [a,1], Kai Jiao [a,1], Qian-Qian Wan [a,1], Jing Li [a], Ming-Yi Liu [a], Zi-Bin Zhang [a], Wen Qin [a], Kai-Yan Wang [a], Ya-zhou Wang [b], Franklin R. Tay [c], Li-Na Niu [a,*]

[a] State Key Laboratory of Military Stomatology & National Clinical Research Center for Oral Diseases & Shaanxi Key Laboratory of Stomatology, School of Stomatology, The Fourth Military Medical University, Xi'an, Shaanxi, 710032, China
[b] Department of Neurobiology, The Fourth Military Medical University, Xi'an, Shaanxi, 710032, China
[c] The Graduate School, Augusta University, Augusta, GA, 30912, USA

ARTICLE INFO

Keywords:
Distal femur defect
Mechanistic target of rapamycin
Semaphorin 3A
Sensory nerve
Silicified collagen scaffolds

ABSTRACT

Sensory nerves promote osteogenesis through the release of neuropeptides. However, the potential application and mechanism in which sensory nerves promote healing of bone defects in the presence of biomaterials remain elusive. The present study identified that new bone formation was more abundantly produced after implantation of silicified collagen scaffolds into defects created in the distal femur of rats. The wound sites were accompanied by extensive nerve innervation and angiogenesis. Sensory nerve dysfunction by capsaicin injection resulted in significant inhibition of silicon-induced osteogenesis in the aforementioned rodent model. Application of extracellular silicon *in vitro* induced axon outgrowth and increased expression of semaphorin 3 A (Sema3A) and semaphorin 4D (Sema4D) in the dorsal root ganglion (DRG), as detected by the upregulation of signaling molecules. Culture medium derived from silicon-stimulated DRG cells promoted proliferation and differentiation of bone marrow mesenchymal stem cells and endothelial progenitor cells. These effects were inhibited by the use of Sema3A neutralizing antibodies but not by Sema4D neutralizing antibodies. Knockdown of Sema3A in DRG blocked silicon-induced osteogenesis and angiogenesis almost completely in a femoral defect rat model, whereas overexpression of Sema3A promoted the silicon-induced phenomena. Activation of "mechanistic target of rapamycin" (mTOR) pathway and increase of Sema3A production were identified in the DRG of rats that were implanted with silicified collagen scaffolds. These findings support the role of silicon in inducing Sema3A production by sensory nerves, which, in turn, stimulates osteogenesis and angiogenesis. Taken together, silicon has therapeutic potential in orthopedic rehabilitation.

1. Introduction

Bone tissue is densely innervated by primary afferent sensory nerve fibers and sympathetic nerve fibers throughout the periosteum, bone marrow and mineralized bone [1]. Anatomical mapping of nerve innervation shows that sensory nerve fibers are the first to be detected in areas with elevated osteogenic activity during skeletal development [2]. Sensory nerves are required for normal vascularization and ossification of endochondral bone [3]. They are also involved in mechanical stimuli adaptation [4] and fracture repair of bone [5]. Moreover, capsaicin-sensitive sensory neurons contribute to skeletal homeostasis and denervation of those neurons reduces new bone formation, with subsequent loss of trabecular connectivity and thickness [6,7]. In the field of bone embryology and traumatology, sensory nerve fibers are predominantly located at metabolically-active regions and are directly involved in osteogenesis through the secretion of neuropeptides. Calcitonin gene-related peptide (CGRP) [8] and substance P (SP) [9] are the most representative neuropeptides involved in osteogenesis. The semaphorins are a highly-conserved family of canonical axon guidance molecules. These molecules were originally identified as axonal growth cone guidance molecules. There is increasing evidence that semaphorins play critical roles in bone homeostasis [10]. While such studies provide

Peer review under responsibility of KeAi Communications Co., Ltd.
* Corresponding author. School of Stomatology, The Fourth Military Medical University, Xi'an, China.
E-mail addresses: niulina831013@126.com, niulina@fmmu.edu.cn (L.-N. Niu).
[1] Equal contributors.

https://doi.org/10.1016/j.bioactmat.2021.07.016
Received 24 April 2021; Received in revised form 12 July 2021; Accepted 17 July 2021
Available online 27 July 2021

circumstantial support for the participation of sensory nerve in bone development and homeostasis, the extent in which sensory nerve-derived signals influence bone regeneration has not been fully elucidated.

Bone defects are caused by a plethora of congenital or acquired conditions. This renders bone the second most transplanted tissue after blood. Natural bone grafts and implants have limitations such as donor scarcity, high resorption rates, disease transfer and immune rejection [11]. In comparison, synthetic biomaterials have distinct advantages in clinical practice because they can be easily sterilized and mass produced [12]. Despite the successful development of bone mimetic materials with physicochemical properties that are similar to those of natural

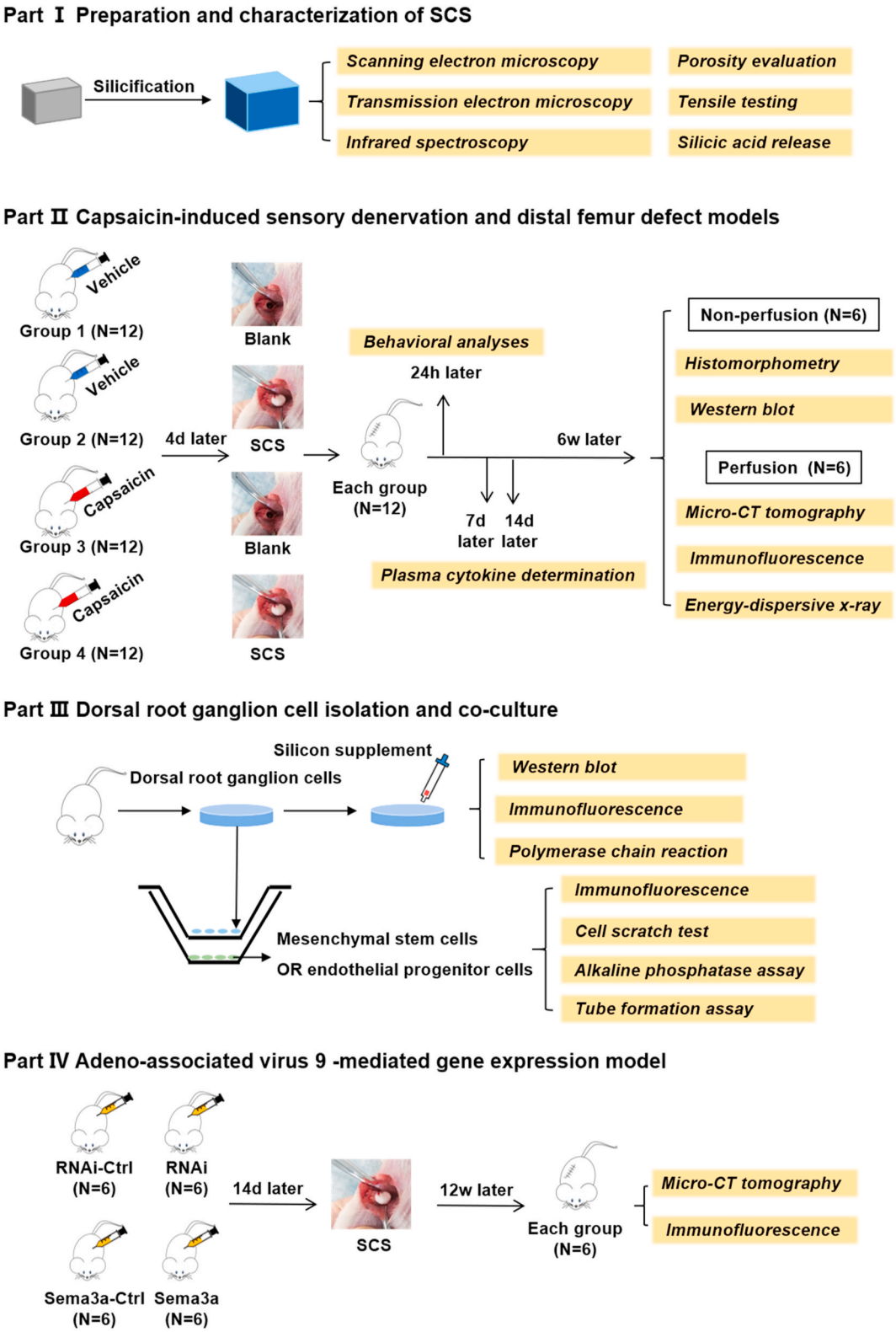

Fig. 1. Flow chart depicting the sequence of experiments conducted in the present study.

bone, most of the bone biomaterials available to date do not induce sufficient formation of blood vessels and nerves. Sensory nerves have been implanted into bone grafts to repair large bone defects. They grow into the pores of the scaffold earlier than the blood vessels and result in better osteogenesis by neurotization [13]. However, surgical implantation of sensory nerves is clinically deterrent because unless approximation of adjacent nerve tracts is achieved, abnormal sensation is inevitable. For this reason, neuropeptides and axonal guidance molecules that possess osteogenic effects have been incorporated into bone scaffolds to promote tissue regeneration. For example, CGRP was used as printing ink in the fabrication of scaffolds and displayed osteoinductive abilities *in vivo* [14]. However, incorporation of proteins into scaffolds creates problems such as short half-lives, high cost, rapid degradation, difficulty in disinfection and immunogenicity. Although magnesium-containing implants promoted repair of femur fracture in osteoporotic rats via increase in CGRP level at the dorsal root ganglion (DRG) [15], the rapid degradation of pure magnesium limited its application in bone tissue engineering. Thus, it is logical to exploit the neurogenic potential of biomaterials in enhancing bone regeneration.

Silicon is an essential trace element for the human body. Adequate silicon (Si) intake is required for bone homeostasis [16]. The success of silicate-based glasses as bioactive materials is attributed to the positive effects of Si on osteoblasts, osteoclasts and endothelial cells [17]. It has been reported that dietary Si supplements help maintain the number of nitrergic neurons and their expression of nitrergic enzymes at physiological levels [18]. Inhalation of Si, a common contaminant in coal mine dust, causes increased substance P synthesis in trigeminal sensory neurons [19]. These results suggest that Si has potentially unresolved effects on the physiology of sensory nerves.

The authors previously reported that silicified collagen scaffolds (SCSs) promote the repair of skull defects in mice [20]. In the present work, SCS synthesis is simplified using choline chloride as pretreating agent and stabilizer for intrafibrillar silicification of collagen matrices. Following their characterization, the effects of choline-induced SCSs on bone regeneration were evaluated using a rat femoral defect model, with specific emphasis on the role of sensory nerves in osteogenesis and angiogenesis. The effect of Si on the phenotype of DRG cells was further examined by screening the expression of several neuropeptides and axonal guidance molecules. A flow chart depicting the sequence of experiments conducted in the present study is included in Fig. 1. The mechanism in which sensory innervation promotes bone formation was delve into for stimulating further research in this largely uncharted terrain.

2. Materials and methods

2.1. Preparation and characterization of SCS

2.1.1. Preparation

A 3 % silicic acid stock solution was prepared by mixing Silbond 40 (partially-hydrolyzed product of tetraethyl silicate with a minimum silica content of 40 wt%; Silbond Corp., Weston, MI, USA), absolute ethanol, water and 37 % HCl in the molar ratios of 1.875: 396.79: 12.03: 0.0218 [21]. Choline-stabilized silicifying medium was prepared from a mixture of the stock solution and 0.07 M choline chloride (MilliporeSigma, St. Louis, MO, USA) in a 2:1 vol ratio. Reconstituted type I collagen tapes (Ace Surgical Supply, Brockton, MA, USA) were cut into 3-mm diameter cylinders and conditioned in 0.07 M choline chloride solution for 2 h. Each expanded collagen cylinder was placed in 5 mL of silicifying medium at 37 °C for 7 days, with daily changing of the medium. The silicified scaffolds were sterilized using cobalt-60 irradiation prior to further investigation.

2.2. Scanning electron microscopy

The specimens were rinsed in distilled water and dehydrated in an ascending ethanol series (50–100 %). Specimens were critical point dried, sputter-coated with gold/palladium and examined using a scanning electron microscope (SEM; Hitachi S-4800, Tokyo, Japan). Elemental analysis of Si was performed using an energy dispersive X-ray analysis (EDXA) detector (AMETEK, Mahwah, NJ, USA). Two-dimensional (2D) porosity and average pore area were calculated using the particle analyzer function of the ImageJ software (National Institute of Health, Bethesda, MD, USA) (n = 6).

2.3. Transmission electron microscopy

Silicified collagen scaffolds were dehydrated in an ascending ethanol series, immersed in propylene oxide and embedded in epoxy resin. Ninety nanometer-thick sections were prepared and examined using a transmission electron microscope (TEM; Tecnai G2, FEI Company, Hillsboro, OR, USA).

2.4. Infrared spectroscopy

Silicified and pristine collagen scaffolds were desiccated with anhydrous calcium sulfate for 24 h prior to spectrum acquisition. Attenuated total reflection-Fourier transform infrared spectroscopy (ATR-FTIR) was performed using a Shimadzu 8400 S spectrometer (Shimadzu Corp., Kyoto, Japan) at ambient temperature from 4000 to 400 cm^{-1}, with 32 scans averaged at a resolution of 4 cm^{-1}. Spectra analysis was performed using IR solution software (Shimadzu).

2.5. Porosity evaluation

Absolute ethanol was used as the displacement liquid for measuring the porosity of SCSs (n = 6). Pre-weighed (Wdry) specimens with known volume (V) were immersed in ethanol for 1 h in vacuum to saturate the pores, after which the specimens were re-weighed (Wsat). Porosity was determined using the formula: (Wsat – Wdry)/(ρV) x 100, where ρ is the density of alcohol.

2.6. Tensile testing

Twelve collagen tapes with dimensions 40 × 8 × 2 mm^2 (length × breadth × height) were cut and a random sample of 6 were silicified. The average thickness of the specimens was calculated from six measurements taken at representative random points with a digital micrometer (Mitutoyo, Kanagawa, Japan). Each specimen was rehydrated in phosphate-buffered saline (MilliporeSigma) and then fixed between the two opposing grips of a tensile tester (Shimadzu). The specimen was stressed to failure using a crosshead speed of 1 mm/min (n = 6). The tensile modulus was determined as the slope of the linear region of the stress-strain curve.

2.7. Silicic acid release

Desiccated SCSs (100 mg each) were soaked in 10 mL ion-free Tris-HCl (pH = 7.4) at 37 °C. At designated time periods (0.125, 0.25, 0.5, 1, 2, 4 and 8 day), 400 μL immersion solutions were retrieved for evaluation of silicic acid release (n = 6). The concentrations of silicic acid were measured by using the silicomolybdic acid spectrophotometric method, based on the ability of silicic acid to form silico-12-molybdic acid in the presence of acidified ammonium heptamolybdate [21].

3. Animal experiments

3.1. Animals

Animal experiments were approved and conducted in accordance with guidelines established by the Institutional Animal Care and Use Committee of the Fourth Military Medical University. Seventy-two Male

Sprague-Dawley rats (200–250 g) were kept under specific-pathogen-free conditions and used for all *in vivo* experiments in the present study. Anesthesia was performed by intraperitoneal injection of sodium pentobarbital (40 mg/kg).

3.2. Dorsal root ganglion exposure

To examine the effect of direct application on dorsal root ganglion (DRG) neurons, the L4/L5 DRG in each rat was exposed by aseptic surgery. A 2 cm-long midline dorsal incision was made over the lumbar spine to expose the ligamentous insertions of the erector spinae group of muscles. Such a procedure enabled the lumbar vertebrae to be identified. Ligamentous attachments to the articular surfaces of the vertebrae were severed to expose the L3-L5 lateral processes, which were removed to reveal the underlying DRG. Capsaicin solution or recombinants virus were then injected directly into the DRG tissue.

3.3. Capsaicin-induced sensory denervation model

Capsaicin-induced selective lesion of sensory fibers in skeletally mature rats has been well described [6,7]. Capsaicin (MilliporeSigma) and vehicle solution (composed of Tween-80, ethanol and saline; volume ratio 1:1:8) were freshly prepared and mixed homogeneously prior to treatment. Twenty-four rats were injected at L3–L5 DRG with the capsaicin-vehicle mix on 3 consecutive days (30 mg/kg on day 1, 50 mg/kg on day 2 and 70 mg/kg on day 3). The other twenty-four rats were injected with vehicle solution only. After capsaicin injection at day 4, the rats were randomly chosen for SCS implantation into the distal femur.

3.4. Viral vector preparation and administration

Recombinant adeno-associated virus 9 (rAAV9) was chosen based on its ability to achieve efficient gene transfer [22]. Four plasmids were designed and constructed using standard methods by Shanghai GeneChem Co. Ltd. (Pudong, Shanghai, China). For *in vivo* RNA interference (RNAi) experiments, small interfering RNA (siRNA) was cloned into a vector containing a U6-promoter multiple cloning sites and enhanced green fluorescent protein (EGFP), and then packaged into the AAV9-RNAi vector (AAV9-Sema3a-RNAi). The AAV9 that expressed siRNA targeting a non-specific sequence (CGCTGAGTACTTCGAAATGTC) was used as control (CON 305). The AAV9-Sema3a was constructed using a vector that contains a cytomegalovirus-promoter driving Sema3a expression and EGFP. Full length complementary DNAs (cDNAs) of Sema3a was transcribed from the Sprague-Dawley rat cDNA library. The AAV9 that expressed promoter and EGFP was used as control (CON 299). Detailed backbone and target sequences are included in the Supplementary Material (SI-1).

Injection of rAAV9 into L3–L5 DRG tissue was performed to overexpress or knockdown Sema3A in the sensory nerves. Twenty-four rats were randomly divided into four groups and then a solution containing 10^{10} genome copies of CON299, CON305, AAV9-Sema3a or AAV9-Sema3a-RNAi was slowly injected using a Hamilton syringe. The glass needle was left in place for 1–2 min prior to its removal to prevent reflux. The muscle layers were then approximated and the skin incision was stapled to facilitate repair. The animals were observed closely postoperatively during recovery. After vector administration at day 14, all rats were prepared for SCS implantation into the distal femur.

3.5. Distal femur defect model

Femur defects in rats were established according to the previously described procedures [23]. A ~1.5 cm lateral linear incision was made in the right distal femoral epiphysis of 48 rats mentioned in the establishment of sensory denervation model and 24 rats in the gene transfer model. This was followed by blunt dissection of the muscle to expose the femoral condyle. A 3 mm diameter, 4 mm deep bone tunnel was created perpendicular to the distal femur using a trephine under constant irrigation with normal saline. A cylindrical shape defect was then prepared after removing the bone fragments. 12 rats injected with capsaicin and 12 rats injected with capsaicin vehicle were implanted with SCS and the incisions were closed layer by layer using resorbable sutures. For the blank group, the defect area was not filled with graft material.

In the present study, two sets of experiments were performed to examine the effect of SCS on bone regeneration. In the first set of experiments, the rats were divided into 4 groups: blank (drill control + vehicle injection), SCS (SCS implantation + vehicle injection), capsaicin + blank (drill control + capsaicin injection) and capsaicin + SCS (SCS implantation + capsaicin injection). In the second set of experiments, the rats were divided into 4 groups: CON299 (SCS implantation + CON299 injection), CON305 (SCS implantation + CON305 injection), AAV9-Sema3a (SCS implantation + AAV9-Sema3a injection) and AAV9-Sema3a-RNAi (SCS implantation + AAV9-Sema3a-RNAi injection). After SCS implantation, the first experimental set of animals were sacrificed on week 6, while the second set of animals were sacrificed on week 12.

3.6. Pain-related behavioral analyses

Pain-related behavioral analyses of rats in the first experimental set were evaluated 24 h after SCS implantation. The rats were placed individually in an opaque acrylic chamber that has a metal mesh floor to enable communication (n = 12). The rats were allowed to accustom to the test environment for 20 min prior to testing [24]. Mechanical withdrawal response was determined using von Frey filaments. The filaments were applied with approximate forces (in g) in ascending order. Three withdrawal tests were performed, each separated by a 10 min test-free period. The lowest force from the 3 tests that produced a response was used to calculate the pain withdrawal threshold. For thermal sensitivity, each rat was placed on a transparent glass plate and acclimatized for 15 min prior to the experiment. The hind paws were stimulated with a radiant heat source (50 W halogen bulb). The time elapsed from initiation of the stimulus until a positive withdrawal response was measured [24]. Each hind paw was tested 3 times at an interval of 10 min. The pain withdrawal latency value was calculated as the mean of the three measurements.

3.7. Plasma cytokine determination

At 7 and 14 days after implantation, the concentrations of plasma inflammatory factors interferon (IFN)-γ, interleukin (IL)-2 and IL-4 in the peripheral circulating blood of the rats (n = 6) were examined with IFN-γ Quantikine ELISA Kit, IL-2 Quantikine ELISA kit, IL-4 Quantikine ELISA kit and, respectively (R&D systems, Minneapolis, MN, USA).

3.8. Micro-computed tomography

The bone specimens were scanned using micro-computed tomography (Micro-CT; Inveon, Siemens Preclinical, Knoxville, TN, USA) at a resolution of 18 μm. A three-dimensional image was reconstructed based on the scanned information using the Inveon Research Workplace software (Siemens Medical Solutions USA, Inc., Hoffman Estates, IL, USA). A cylindrical region of interest was positioned over the defect site and the volume of the newly-formed bone was measured by assigning a threshold. Bone volume to total volume ratio (BV/TV), bone mineral density (BMD) and trabecular thickness (Tb. Th) in the defects were measured using the Inveon Research Acquisition software.

3.9. Histology and histomorphometry

Calcein green (5 mg/kg, MilliporeSigma) was administered intraperitoneally to rats in the first experimental set 7 days prior to

euthanasia to label the newly-formed bone (n = 6). On the day of sacrifice, femoral condyles were retrieved from each group and fixed with 4 % neutral formaldehyde. After dehydration through an ethanol series, the chemically-dehydrated specimens were infiltrated with purified methyl methacrylate, which was then polymerized. The embedded, undecalcified specimens were sectioned longitudinally at a thickness of ~50 μm (Leica SP1600, Mannheim, Germany). The undecalcified sections were stained with von Kossa stain (Servicebio, Wuhan, Hubei, China) to analyze morphological changes in the defect sites. Images of sections labeled with calcein green were taken on the margin of defect to observe the rate of new bone tissue formation. Measurements and calculations for static and dynamic histomorphometry were accomplished using the ImageJ software (National Institute of Health, Bethesda, MD, USA).

3.10. Western blot

Western blot assay was used to identify the expression or phosphorylation of DRG tissues derived from the SCS and the blank groups that were sacrificed on week 6 (n = 6). Previous studies have shown that Si activates Wnt/β-catenin [25], MAPK/p38 [26] and PI3K/Akt/mTOR signaling pathways [27]. Freshly separated tissues were homogenized and lysed in radio-immunoprecipitation assay lysis containing 1x phosphatase inhibitor cocktail (Roche, Mannheim, Germany). The lysate was centrifuged and the supernatant was collected for total protein concentration determination using Pierce BCA protein assay kit (Solarbio, Beijing, China). Protein samples were separated with a 10 % SDS-polyacrylamide gel and transferred onto a polyvinylidene difluoride membrane (EMD Millipore Corp., Billerica, MA, USA). The membrane was blocked with 5 % nonfat milk and incubated for 3 h. Signals were revealed after incubation with horseradish peroxidase-conjugated secondary antibody (Santa Cruz) and enhanced chemiluminescence detection (GeneTex, Irvine, CA, USA). The stained bands were scanned and quantified using a densitometer (Tanon, Shanghai, China) and ImageJ software. Protein expression levels were normalized against β-actin.

The following primary antibodies were used: active-β-catenin (8814, Cell Signaling Technologies), β-catenin (9562, Cell Signaling Technologies), p38 MAPK (9212, Cell Signaling Technologies), phospho-p38 MAPK (9211, Cell Signaling Technologies), PI3 Kinase p85 (4257, Cell Signaling Technologies), Phospho-PI3 Kinase p85 (17366, Cell Signaling Technologies), phospho-Akt (4060; Cell Signaling Technologies), AKT antibody (GTX121937, GeneTex), mTOR antibody (GTX101557, GeneTex), phospho-mTOR (Ser2481) (2974, Cell Signaling Technologies), semaphorin 3 A antibody (sc-74555, Santa Cruz Biotechnology) and actin (GTX11003, GeneTex).

4. Dorsal root ganglion cell isolation and co-culture

The cell bodies of afferent nerves are generally positioned in the dorsal root ganglia (DRG). Neonatal Sprague-Dawley rats (1–5 day old) were decapitated and their DRGs were aseptically dissected from all spinal levels. The isolated tissue was digested with 0.1 % collagenase (MilliporeSigma) and 0.25 % trypsin (Invitrogen, Thermo Fisher Scientific). The isolated cells were re-suspended in Neurobasal-A medium (Invitrogen) containing 0.5 mM L-glutamine (LG), penicillin-streptomycin (PS; 1:100, MilliporeSigma) and 2 % B-27 (Invitrogen) at a density of 10,000 cells/mL. The harvested DRG cells were planted on round-glass slices or the upper chamber of 24-well Transwell (0.4 μm pore size, Corning Life Sciences, Lowell, MA, USA) coated with poly-*d*-lysine hydrobromide (50 ng/mL, Thermo Fisher Scientific). After 4 h, the culture medium was replaced with Neurobasal-A/LG/PS/B-27 medium and 20 ng/mL nerve growth factor (NGF; MilliporeSigma). The cells were allowed to differentiate for 3–5 days at 37 °C with 5 % CO_2 and 95 % air in a humidified incubator. The medium was changed every other day. The DRG neurons were further investigated by culturing them for up to 3 days with silicon supplemented medium. Silicon supplemented medium was prepared fresh by diluting the appropriate amounts of sodium orthosilicate (MilliporeSigma) in complete growth medium to obtain final Si concentrations between 5 μM and 40 μM Si.

The use of Transwell cell inserts enabled the DRG cells to share the same growth medium with other cells but had no direct contact. Cells cultured in the lower chamber were mesenchymal stem cells (MSCs; Cyagen Biosciences, Guangzhou, Guangdong, China) or endothelial progenitor cells (EPCs; Jennio Biotech, Guangzhou, Guangdong, China) derived from Sprague-Dawley rats. The MSCs or EPCs were first cultured in Dulbecco's modified Eagle medium (DMEM) supplemented with 10 % fetal bovine serum (FBS), 1 % L-glutamine and 2 % 100 U/mL penicillin and 100 mg/mL streptomycin. For subsequent experiments, Transwell inserts with DRG cells and/or 10 μM silicon-supplemented DMEM were added.

The MSCs or EPCs co-culture system were divided into 6 groups: NC (negative control), Si (silicon supplemented medium), DRG (co-cultured with DRG cells), Si + DRG (co-cultured with DRG cells in silicon supplemented medium), anti-Sema3A (co-cultured with DRG cells in silicon supplemented medium in the presence of Sema3A antibody) and anti-Sema4D (co-cultured with DRG cells in silicon supplemented medium in the presence of Sema4D antibody). The blocking antibodies used were: semaphorin 3 A antibody (sc-74555, Santa Cruz Biotechnology) or semaphorin 4D antibody (sc-136250, Santa Cruz Biotechnology).

4.1. Quantitative real-time polymerase chain reaction

To investigate the temporal relation between SCS stimulation and DRG secretion, gene and protein expressions of CGRP, SP and semaphorins of the DRG cultured in silicon-conditioned medium were evaluated with real-time polymerase chain reaction (n = 6). Briefly, total RNA was isolated using Trizol reagent (Invitrogen). The concentration and purity of the extracted RNA were determined by measuring the absorbance at 260 and 280 nm (BioTek, Winooski, VT, USA). Complementary DNA (cDNA) was synthesized using the PrimeScript RT reagent kit (Takara Bio Inc., Shiga, Japan). The RT-PCR experiment was performed using a 7500 Real Time PCR System (Applied Biosystems, Carlsbard, CA, USA). Sense and antisense primers were designed based on published cDNA sequences using Primer Express 5.0 (Supplementary Material). Glyceraldehyde 3-phosphate dehydrogenase (GADPH) was used as the housekeeping gene. Results obtained after calibration with the GADPH expression level were calculated using the $2^{-\Delta\Delta Ct}$ method and presented as fold increases relative to the non-stimulated control.

4.2. CCK-8 assay

Cell viability of MSCs or EPCs were estimated using the CCK-8 assay (KeyGen Biotech, Nanjing, Jiangsu, China). Working solution with 10 % CCK-8 reagent was added to each well and incubated in the dark for 2 h. Absorbance was measured at 450 nm using a Synergy 2 SL multi-mode microplate reader (BioTek Instruments Inc., Winooski, VT, USA).

4.3. Cell scratch test

When MSC-seeded or EPC-seeded 6-well plates reached confluency, a straight scratch was made using a sterile 10 μL pipette tip. The cells were then incubated with FBS-free culture medium alone or different conditioned media. Images of the scratches were captured after 24 h. The width of the scratches was analyzed using ImageJ software.

4.4. Alkaline phosphatase assay

MSCs placed in the lower chamber were cultured in osteogenic differentiation medium for 14 days, with change of the conditioned medium every 3 days. Alkaline phosphatase (ALP) activity was determined using an ALP assay kit (BioAssay Systems, Hayward, CA, USA). Activity

was calculated by evaluating the absorbance at 520 nm.

4.5. Tube formation assay

The effect of conditioned medium on tube formation from EPCs was evaluated using Matrigel® matrix (Corning). Matrigel was applied to well plates and incubated at 37 °C for 30 min prior to cell seeding. The EPCs were seeded on the polymerized Matrigel and incubated in different conditioned media according to the group designation, at 37 °C for 6 h. Tube formation was examined using light microscopy and the cumulative tube lengths were measured using ImageJ software.

5. Immunofluorescence

For immunofluorescence staining, rats of all groups were euthanized and perfused with heparin sodium (100 U/mL) containing 0.9 % saline (n = 6). Following euthanization, the vasculature was perfused 4 % paraformaldehyde. Dorsal root ganglion (DRG) tissues were post-fixed with 1.5 % glutaraldehyde for 6 h and cryo-protected with 30 % sucrose solution at 4 °C for 24 h. The femurs were post-fixed overnight and decalcified with 10 % ethylenediaminetetraacetic acid (EDTA; pH 7.3) for 3 weeks, with changing of the demineralization medium twice per week. After decalcification, the femurs were cryo-protected with 30 % sucrose solution at 4 °C for 48 h. The DRG tissues and femurs were embedded in optimal cutting temperature compound and incubated overnight at 4 °C. For DRG neurons isolated from neonatal rats, the cells were plated on coverslips and fixed with 4 % paraformaldehyde for 10 min before immunofluorescent imaging. The double-labeled images were captured using a fluorescence microscope (FV1000, Olympus, Japan). Integrated fluorescence intensity was analyzed by the ImageJ software (n = 6). Five fields of view were randomly selected for each specimen for determining the mean fluorescence intensity.

The cryo-sections (15 μm-thick) and cell-laden coverslips were stained using standard immunofluorescence methods. Briefly, the specimens were permeabilized with 0.1 % Triton X-100 (MilliporeSigma) and blocked in 5 % normal donkey serum (Jackson ImmunoResearch, West Grove, PA, USA). The sections were incubated overnight with the primary antibodies at 4 °C. This was followed by incubation with Alexa Fluor™ fluorescent secondary antibodies (Jackson ImmunoResearch, West Grove, PA, USA). All specimens were rinsed and mounted with Prolong Diamond Antifade Mountant with 4',6-diamidino-2-phenylindole (DAPI; Invitrogen, San Diego, CA, USA).

For bone tissue, CGRP is a well-known sensory nerve marker associated with osteogenesis [28]. Leptin receptor (LepR)-expressing mesenchymal stromal cells represent the main source of bone formation originating from adult bone marrow [29]. CD31+Endomucin (Emcn)+ vessels are believed to couple angiogenesis and osteogenesis [30]. Accordingly, sensory nerve distribution and frequency were investigated by LepR, CD31 and Emcn staining at the site of new bone formation using tissue sections derived from the aforementioned four groups. For DRG, hexaribonucleotide binding protein-3 (NeuN) is a specific marker for neuronal soma and the distribution of beta–III–tubulin is almost exclusively neurites specific [31]. The primary antibodies used were: CGRP antibody (ab36001, Abcam; 14959, Cell Signaling Technology, Inc. Danvers, MA, USA), LepR antibody (PA5-18522, Thermo Fisher Scientific, Waltham, MA, USA), PECAM-1/CD31 antibody (sc-376764, Santa Cruz Biotechnology, Inc., Dallas, TX, USA), Emcn antibody (343158, United States Biological, Salem, MA, USA), NeuN antibody (ab177487, Abcam), beta III tubulin antibody (ab78078, Abcam), semaphorin 3 A antibody (sc-74555, Santa Cruz Biotechnology) and semaphorin 4D antibody (sc-136250, Santa Cruz Biotechnology).

6. Statistical analyses

All surgical procedures as well as quantitative histological and behavioral analyses were conducted in a blinded fashion. All data were presented as means ± standard deviations. Data were examined for their normality and homoscedasticity assumptions prior to the use of parametric statistical methods. If those assumptions appeared to be violated, the data were non-linearly transformed to satisfy those assumptions prior to the use of parametric statistical methods. Comparisons between 2 groups were examined using Student's t-test. Comparisons involving more than 2 groups were analyzed using one-factor analysis of variance and post-hoc Tukey's pairwise comparison procedures, after ascertaining that the normality and homoscedasticity assumptions of the corresponding data sets were not violated. The GraphPad Prism 5 package (GraphPad Software, La Jolla, CA, USA) was employed for analysis. Statistical significance was preset at $\alpha = 0.05$.

7. Results

7.1. Characterization of choline-induced SCS

Reconstituted type I collagen scaffolds were heavily silicified after incubation in choline-stabilized silicic acid for 7 days, even without poly (allylamine) hydrochloride pretreatment. When examined with SEM and EDAX, SCSs showed clear evidence of extrafibrillar mineral deposition (Fig. 2A), with increase in silicon content (Fig. 2B, $p < 0.0001$). Intrafibrillar silicification, on the other hand, could only be visualized using TEM (Fig. 2C). The presence of Si–O–Si peaks within the SCS was confirmed using ATR-FTIR (Fig. 2D). Peaks at 1041 cm^{-1}, 802 cm^{-1} and 453 cm^{-1} are assigned to the three main peaks characteristic of Si–O–Si vibrational modes. The silica peak at 960 cm^{-1} associated with silicified collagen is attributed to the Si–OH stretching vibration of hydrated amorphous silica. The ultrastructural features of the SCS revealed intrafibrillar and extrafibrillar silica accumulation that is akin to the biomineralization of carbonated apatite within native bone.[17] Sustained release of silicic acid occurred in SCSs that were immersed in Tris-HCL with a burst release phase during the first 4 days and a stable release phase thereafter (Fig. 2E). The SCSs had a porosity of 86.7 ± 1.5 %, which was significantly higher than unmineralized collagen scaffolds (76.8 ± 2.4 %) (Fig. 2F, $p < 0.0001$). The SCS showed significant increases in 2D porosity and average pore diameter (SI-2). The tensile modulus of SCS was 5.96 ± 0.73 MPa, which was significantly higher than unmineralized collagen scaffolds (2.88 ± 0.51 MPa) (Fig. 2G, $p < 0.0001$). Representative plots of the stress-strain relationships of CS and SCS are shown in SI-3. Compared with native collagen scaffolds, the SCS possessed improved porosity and tensile properties. The increased scaffold volume after silicification created a high degree of porosity. In addition, deposition of intrafibrillar silica enhanced the mechanical strength of the collagen matrix, thereby increasing the tensile modulus.

7.2. Promotion of in-situ bone regeneration by SCSs via sensory nerve innervation

No obvious swelling, purulence or fistula was observed in the four groups 1) blank; 2) SCS; 3) capsaicin + blank and 4) capsaicin + SCS. The plasma levels of IFN-γ, IL-2 and IL-4 between the SCS-implanted group and the blank control group were not significantly different at 7 days or 14 days ($p > 0.05$ for all comparisons) (SI-4). Micro-computed tomography showed that considerable amount of newly-formed bone extended from the periphery to the center of the defects in the SCS and capsaicin + SCS groups (Fig. 3A and B). Conversely, defects in the blank and capsaicin + blank groups had no appreciable bone formation, with a clear boundary of the defect area.

Quantitative analysis showed that BV/TV, Tb.Th and BMD values from the SCS group were significantly higher than those of the other three groups ($p < 0.05$ for all comparisons). In the capsaicin + SCS group, BV/TV, Tb.Th and BMD were significantly reduced compared with the SCS group; the results suggest that sensory innervation plays an important role in bone regeneration. In the absence of SCS implantation, bone regeneration is slower and the effect of sensory nerve dysfunction

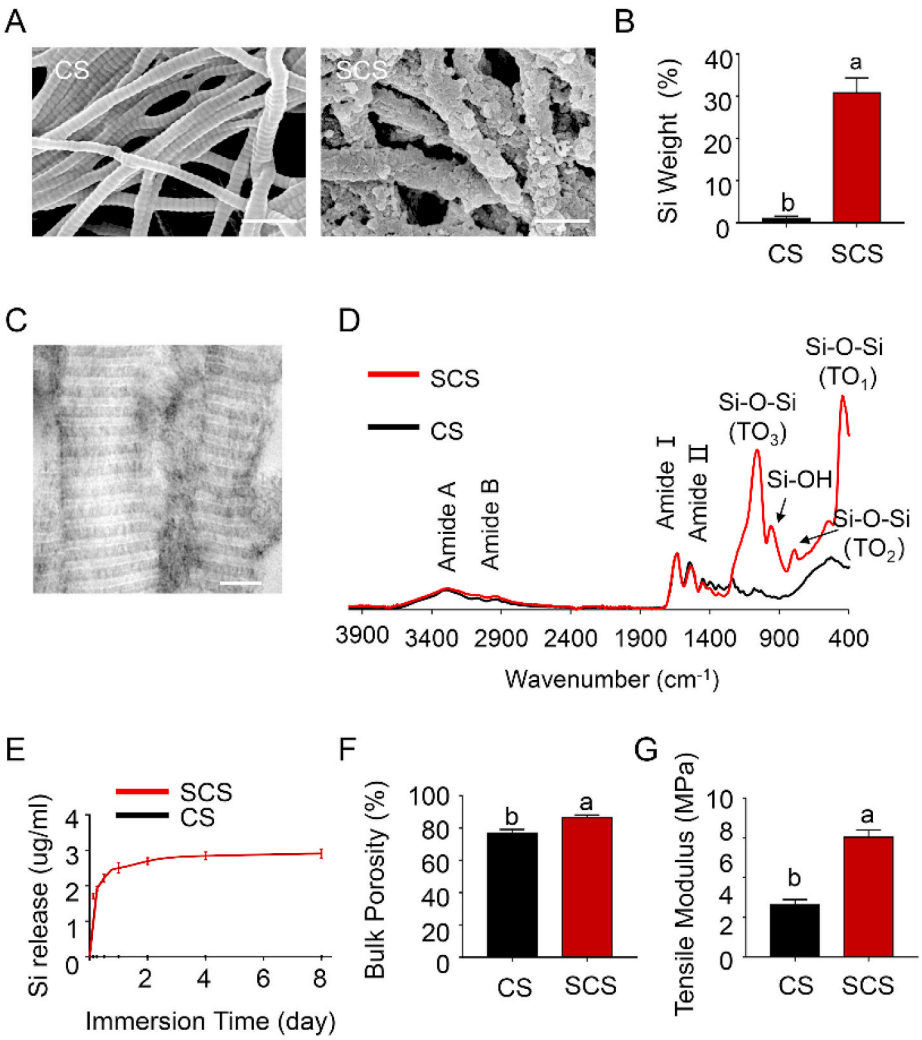

Fig. 2. Characteristics of choline-induced SCS. (**A**) SEM images of collagen scaffold (CS) and silicified collagen scaffold (SCS). Extrafibrillar mineral formation resulted in a crust-like appearance. Scale bar: 500 nm. (**B**) Elemental analysis identified the presence of Si in mineralized specimens and absence of this element in the non-mineralized control (n = 6). (**C**) Unstained TEM images of SCS showed intrafibrillar electron-dense minerals that replicated the cross-banding and microfibrillar architecture of fibrillar collagen. Scale bar: 200 nm. (**D**) Infrared spectra showed amide I (~1635 cm^{-1}) and amide II (~1527 cm^{-1}) peaks that are characteristic of collagen. The SCS and CS spectra are normalized along their amide I peak. (**E**) Accumulative release of silicic acid in Tris-HCl at different time points (n = 6). (**F**) Porosity and (**G**) tensile moduli of the different scaffolds (n = 6). Data represent means ± standard deviations. For all charts, groups labeled with different lowercase letters are significantly different ($p < 0.05$).

is also weakened. von Kossa staining (Fig. 3C and D) and *in vivo* calcein labeling (Fig. 3E and F) showed similar results, reflecting the critical role played by sensory nerves for SCS-promoted bone regeneration.

Bone-associated nerves and blood vessels are thought to influence the propagation of one another as they grow within bone tissues. To clarify this issue, immunofluorescence staining was conducted to examine the potential relationship between the sensory innervation and the enhanced angiogenesis and osteogenesis. The results showed that CGRP + sensory nerve co-localized respectively with LepR + MSC and CD31+Emcn + vessels in areas of new bone formation in the SCS and capsaicin + SCS groups (Fig. 4). Significantly more CGRP + sensory nerve, CD31+Emcn + vessels and LepR + MSC were identified in the SCS group when compared with the other groups. Compared with the SCS group, expressions of sensory fibers, blood vessels and MSCs were significantly reduced in the capsaicin-SCS group. There was no significant difference between the capsaicin treatment group and the blank group. The expression level of CGRP, LepR, CD31 and Emcn in the capsaicin-blank group was the lowest. Taken together, the results infer that sensory nerve innervation, vascularization and MSC homing of bone defects follow a closely-related pattern. Increase in sensory nerve innervation coincides with vascularization and ossification.

To examine whether Si-stimulated sensory nerves in bone repair alter pain sensation, mechanical and thermal withdrawal responses were conducted one day post-surgery. (SI-5) There were no significant changes in pain withdrawal responses between the groups of animals receiving blank or SCS implantation. These findings suggest that SCS implantation was not adversely accompanied by mechanical allodynia and thermal hyperalgesia. In contrast, pain withdrawal latency was significantly increased after capsaicin treatment. The capsaicin results were confirmative of a successful sensory denervation model.

7.3. *Silicon promotes DRG axonal growth and secretion of semaphoring 3 A in vitro*

Doral root ganglion tissues in the SCS and capsaicin + SCS groups contained a higher level of Si than those in the blank and capsaicin + blank groups (SI-6). Nevertheless, the role of silicic acid in the peripheral sensory nervous system during bone repair remains obscure. The DRG neurons were isolated from neonatal rats for further investigation, by culturing them for up to 3 days with various concentrations of silicon supplemented medium Immunofluorescence was performed using anti-β-III tubulin and anti-NeuN antibodies (Fig. 5A). Silicon below 10 μM did not suppress neurite growth or neuron survival remarkably. Indeed, an appropriate concentration of Si (5 or 10 μM) was required to promote axonal elongation of DRG cells. This observation was further supported by quantitative analyses of cell count (Fig. 5B) and neurite assays (Fig. 5C).

To investigate the effects of Si on DRG secretion, RT-PCR and immunofluorescence staining were used to detect different families of neuropeptides and axonal guidance molecules. Silicon supplemented noticeably elevated expression of the associated genes derived from DRG, compared with the blank control. Expressions of Sema3A and

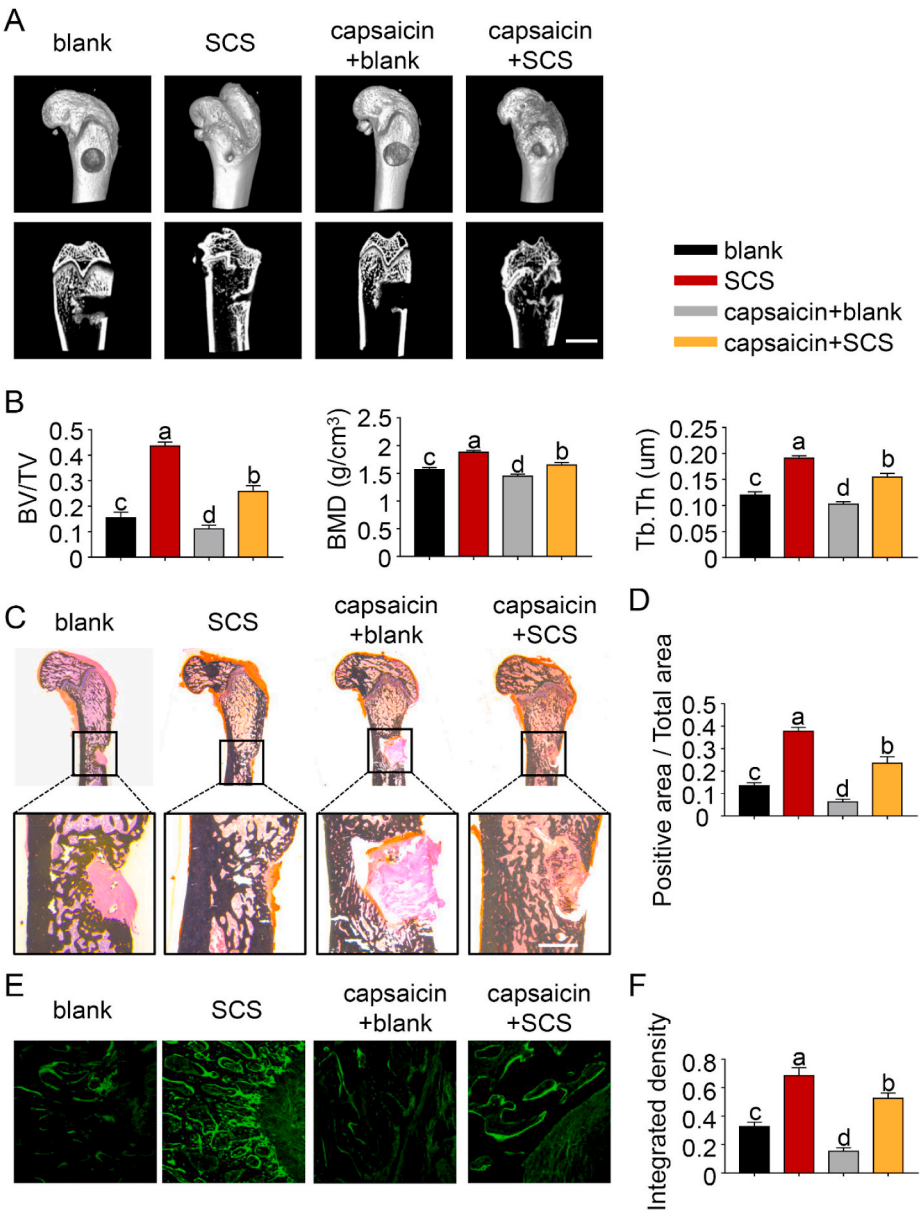

Fig. 3. SCS promotes bone regeneration via sensory nerve innervation. (**A**) Representative micro-CT images of 3D-reconstructed superficial and interior images of distal femoral defects 6 weeks after SCS or blank implantation, with or without capsaicin treatment. Scale bar: 4 cm. (**B**) Quantitative analysis of bone volume/total volume (TV/BV), bone mineral density (BMD) and trabecular thickness (Tb.Th) (n = 6). (**C**) von Kossa silver staining for new bone. Scale bar: 2 cm. (**D**) Bar chart depicting the von Kossa silver staining results (n = 6). (**E**) Calcein labeling for new bone. Scale bar: 100 μm. (**F**) Bar chart depicting the calcein labeling results (n = 6). For all charts, data represent means ± standard deviations; groups labeled with different lowercase letters are significantly different ($p < 0.05$).

Sema4D RNA were significantly increased when silicate was used to stimulate DRG *in vitro* ($p < 0.0001$ for Sema3A; $p = 0.0029$ for Sema4D). By comparison, RNA expressions of CGRP, SP, Sema3E and Sema7D were not significantly different from the blank control (Fig. 5D). Because semaphorins are extensively expressed by DRG neurons, immunofluorescence staining was used to confirm the presence of semaphorins and β-III tubulin in isolated DRG neurons (Fig. 5E). In the absence of Si in the staining bath, Sema3A was seen almost exclusively at neuronal terminals. Upon the addition of Si, Sema3A intensity in the neuron bodies was increased within 24 h ($p < 0.0001$). However, no significant change was found in the expression of Sema4D ($p > 0.05$). Taken together, the results support that Si promotes DRG axonal growth and Sema3A expression *in vitro*.

7.4. Silicon-stimulated DRG promotes MSC/EPC homing, osteogenesis and angiogenesis

The responses of MSCs and EPCs to different culture media were investigated to probe the mechanism of Si-stimulated DRGs in promoting osteogenesis and angiogenesis *in vitro*. The effects of Si-stimulated DRG on MSCs and EPCs were quantified using CCK8 assay and cell scratch assay (Fig. 6A, D). The results indicate that culture medium conditioned with only DRG or Si did not stimulate proliferation and migration of MSCs or EPCs after 24 h ($p > 0.05$). In contrast, proliferation and migration of MSCs and EPCs increased significantly in the culture medium that had been conditioned with Si-stimulated DRG ($p < 0.0001$).

In vitro osteogenesis was performed at co-culture day 14 to analyze the effect of DRG on osteogenic differentiation of MSCs. Alkaline phosphatase is an early marker for osteoblast lineage development. The result showed that MSCs co-cultured with Si-stimulated DRG neurons for 14 days exhibited more intense staining for ALP (Fig. 6B). Identical results were achieved when the ALP activity was quantified (Fig. 6C, $p < 0.05$).

The effect of co-culture medium on *in vitro* angiogenesis was performed using tube formation, which is a simplified model of angiogenesis evaluation. Endothelial progenitor cells co-cultured with Si-stimulated DRG induced cell migration and alignment, followed by the development of capillary-like tubes and sprouting of new capillaries (Fig. 6E). Tube length of the network structure induced by Si-stimulated

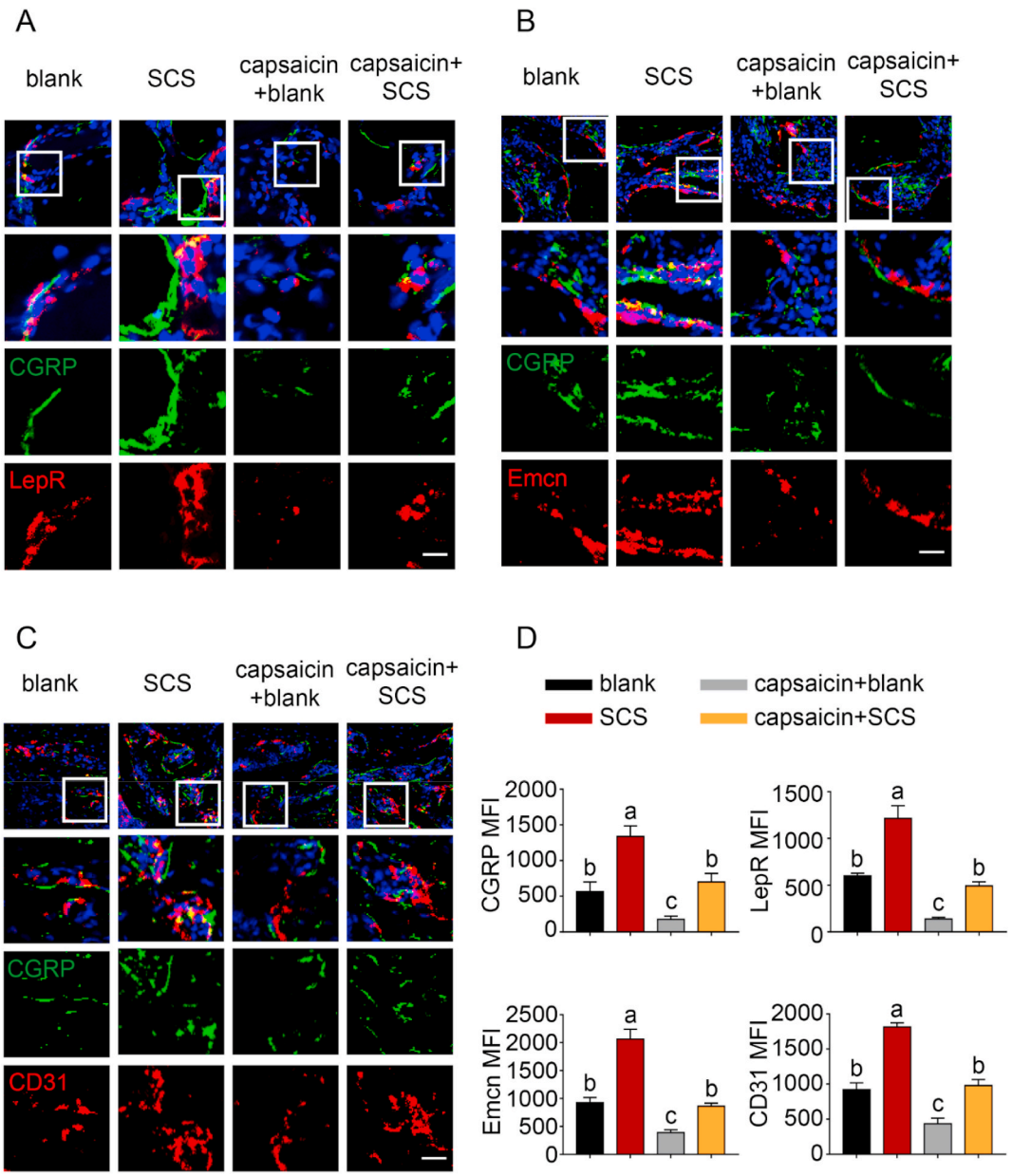

Fig. 4. Immunofluorescence staining of defect areas at 6 weeks after surgery. (**A**) Representative images of immunofluorescence staining of CGRP and LepR. (**B**) Representative images of CGRP and Emcn staining. (**C**) Representative images of CGRP and CD31 staining. (**D**) Quantification of CGRP, LepR, Emcn and CD31 median fluorescence intensity (MFI) per field view. Nuclei were stained with DAPI (blue). Scale bar: 100 μm. Data represent means ± standard deviations (n = 6). For all charts, groups labeled with different lowercase letters are significantly different ($p < 0.05$).

DRG was significantly longer than the other groups (Fig. 6F, $p < 0.05$).

The effect of Si or DRG cells alone on osteogenesis or angiogenesis is not as effective as that of Si-stimulated DRG. Conspicuously, the effects of Si-stimulated DRG on osteoblast differentiation and tube formation were blocked after incubation with Sema3A neutralizing antibody instead of Sema4D antibody (Fig. 6C, F, $p < 0.05$). In particular, Sema4D mainly exists as membrane proteins, and only a small amount functions in secretory. Previous studies have confirmed that neutralizing antibody can effectively block the regulatory activity of Sema4D in cell culture and animal models [32]. Taken together, the data suggest that Si-stimulated DRG regulates osteoinduction of MSCs and pro-angiogenesis of EPCs. This, in turn, results in better extrafibrillar mineralization and capillary formation. The upregulation of osteogenic/angiogenic phenotypes also indicate that bone regeneration is associated with neural production of Sema3A.

7.5. Sema3A promotes osteogenesis and angiogenesis in SCS-mediated bone regeneration

To further confirm the involvement of Sema3A in Si-induced osteogenesis, direct intra-DRG injection of AAV9-Sema3a or AAV9-Sema3a-RNAi was performed to overexpress or knockdown Sema3A in the sensory nerves. All animals recovered within 3 h after operation and showed no apparent abnormal behavior after rAAV9 treatment. Immunofluorescence staining confirmed successful transduction of rAAV9 in DRG neurons *in vivo* (SI-7). For osteogenesis evaluation, micro-CT reconstruction was performed after 12 weeks of implantation (Fig. 7A). The 3D images clearly depicted differences among groups. Significantly more bone volume was observed in the AAV9-Sema3a group; the defects were almost fully-healed, with the appearance of new plate-like bone patterns peripherally and centrally. Commensurate with the image observations, the RNAi group had the lowest BV/TV,

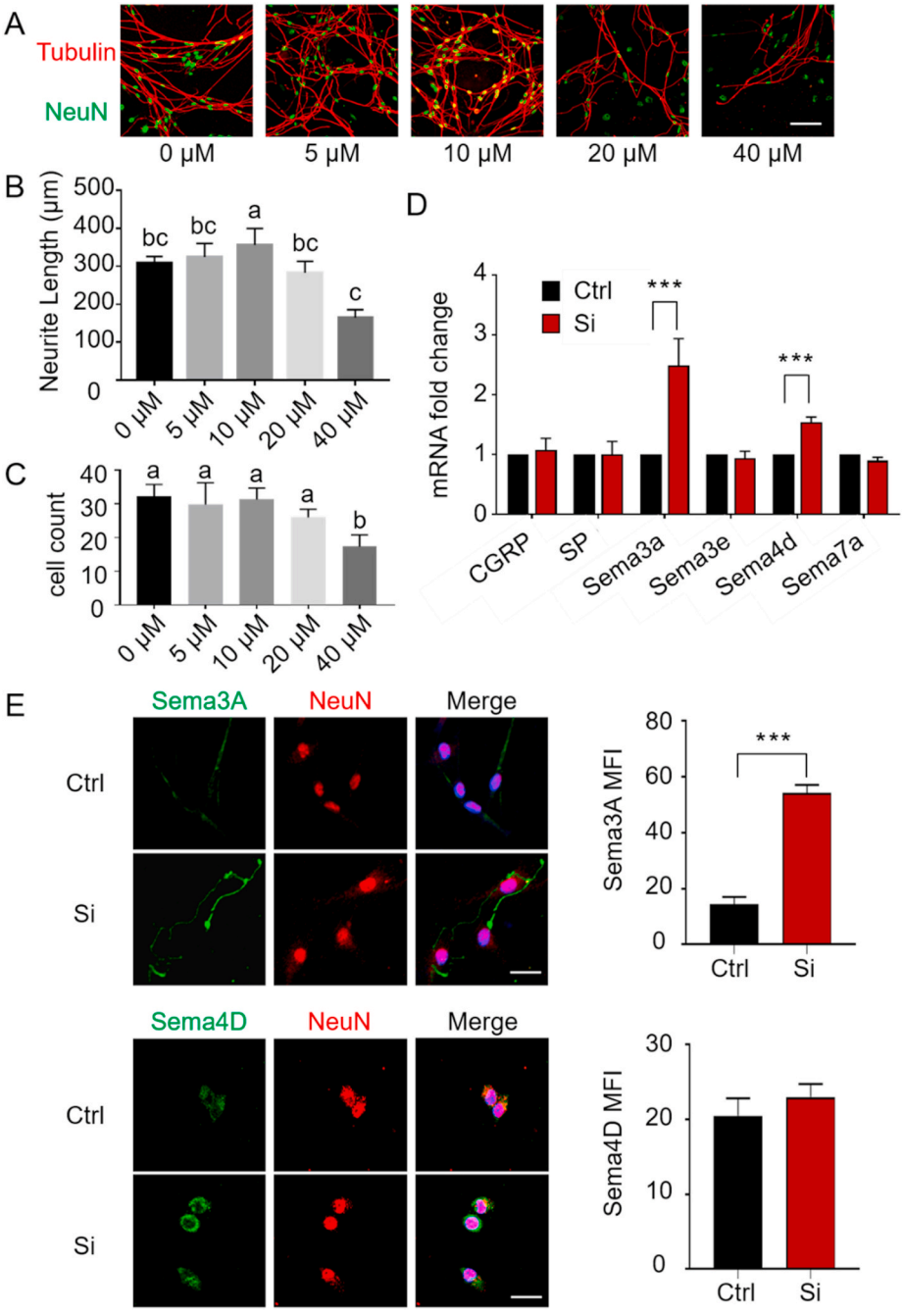

Fig. 5. Si promotes DRG axonal growth and secretion of semaphorins *in vitro*. (**A**) Representative immunofluorescence images of DRG neurons cultured with various concentrations of Si for 2 days. Scale bar: 200 μm. Green: anti-β-III tubulin antibody. Red: anti-NeuN antibody. Quantitative analyses of neurite length (**B**) and neuron survival (**C**) under indicated treatments, respectively (n = 8). (**D**) Real-time PCR was performed using primers targeting the neuropeptides and axonal guidance molecules in DRGs exposed to 10 μM Si. Increased levels of semaphorin expression were detected in their DRGs compared with control (n = 3). (**E**) Representative double-immunofluorescent staining of NeuN (red), Sema3A (green) and Sema4D (green) in DRG neurons with quantification of MFI per field view (n = 8). Scale bar: 50 μm. Data represent means ± standard deviations. For all charts, groups labeled with *** ($p < 0.001$) or different lowercase letters ($p < 0.05$) are significantly different.

BMD and Tb.Th values among all groups (Fig. 7B, $p < 0.05$). Compared with control groups, significantly higher BV/TV, BMD and Tb.Th values were recorded in SCS-implanted defects with AAV9-Sema3a injection ($p < 0.05$). Conversely, significantly lower bone parameter values were recorded in defects associated with AAV9-Sema3a-RNAi injection ($p < 0.05$). Quantitative micro-CT analysis revealed no detectable changes among control groups ($p > 0.05$). The results indicate that neural Sema3A production initiated by SCS promotes bone regeneration *in vivo*, confirming the results of *in vitro* evaluation.

Specimens stained with CGRP, LepR, Emcn and CD31 enabled simultaneous visualization of the location of sensory nerves, MSCs and capillaries (Fig. 7C–F). Defects in the AAV9-Sema3a group were filled with significantly more $CGRP^+$ nerve fibers ($p < 0.05$). Likewise, $LepR^+$ cells were prominently identified in the AV9-Sema3a group ($p < 0.05$). The AAV9-Sema3a group also showed a large number of $CD31^+$ and $Emcn^+$ vessels than the other groups ($p < 0.05$). In addition, the change in $CGRP^+$ fiber frequency closely mirrored those of $LepR^+$ cells, $CD31^+$ vessels and $Emcn^+$ vessels. Taken together, the results indicate that Sema3A production is closely associated with sensory nerve innervation and blood vessel formation during osteogenesis.

7.6. Silicon up-regulates DRG Sema3A expression by activating Akt-mTOR signaling

The signaling pathway involved in silicon upregulation of DRG Sema3A expression was the last to be investigated. Expression of Sema3A was improved for the DRG tissues obtained from the SCS group, compared with the blank control (SI-8). Western blot of the Wnt/β-catenin and MAPK/p38 pathways showed no obvious changes. Expressions of phosphorylated PI3K, Akt and mechanistic target of

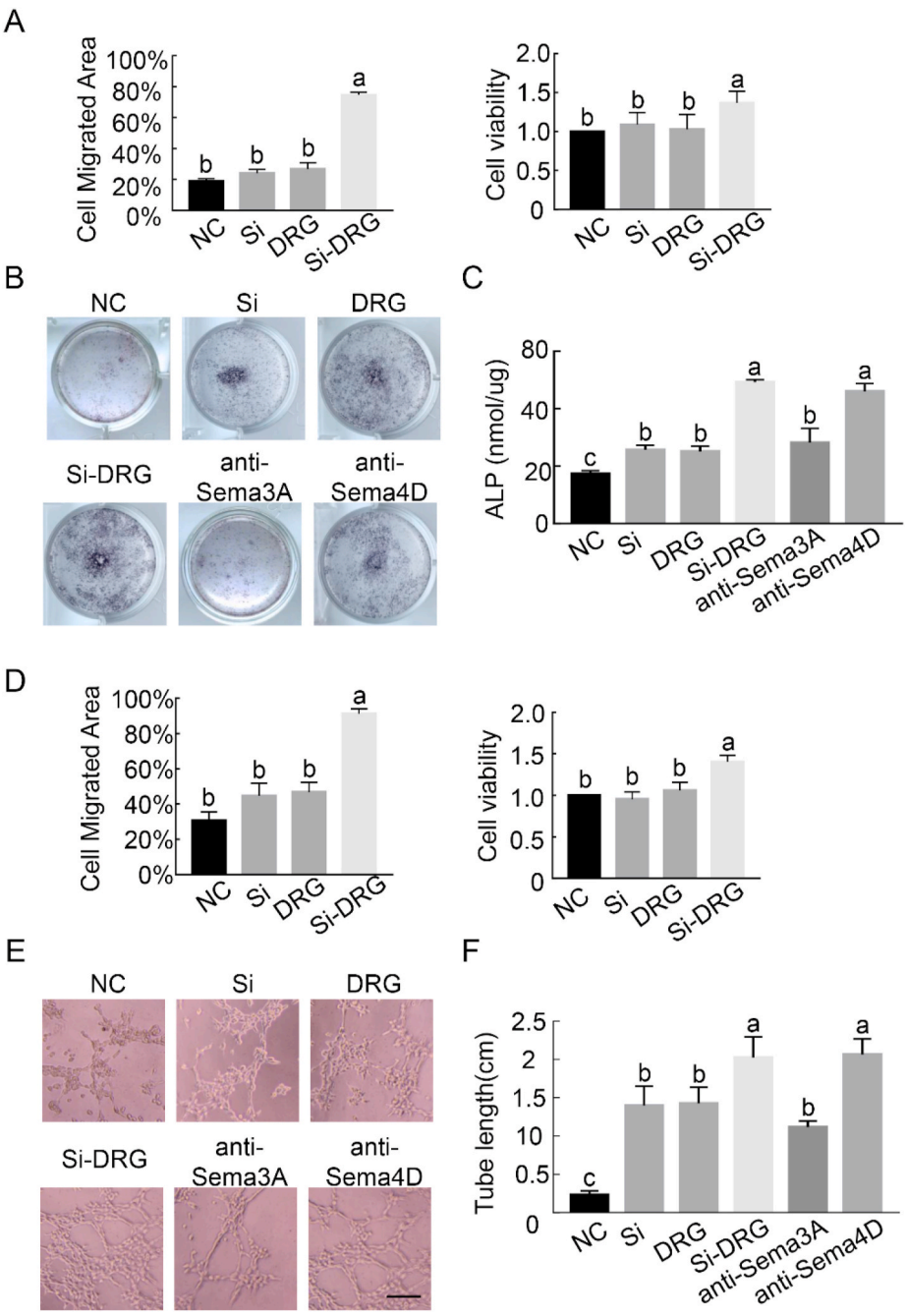

Fig. 6. Silicon-stimulated DRGs promote MSC/EPC homing, osteogenesis and angiogenesis by semaphorin 3 A. Results of *in vitro* assays were performed in different conditioned media groups. (A) The stimulatory effect of Si-stimulated DRGs on MSC proliferation and migration. Quantitative analysis of CCK8and scratch-wound healing assays was performed at 24 h. (**B**) Representative light microscopy images show alkaline phosphatase (ALP) staining at 7 days in the presence of neutralizing antibodies. (**C**) ALP activity in MSCs was analyzed quantitatively. (**D**) The invigorating effect of Si-stimulated DRG extracts on proliferation and migration of EPCs. Summary of CCK8 and scratch-wound healing assays was performed at 24 h. (**E**) Representative light microscopy images show tube formation in the presence of neutralizing antibodies for 6 h. Scale bar: 100 μm. (**F**) Quantitative analysis of *in vitro* angiogenesis by measuring the area occupied by the tubular structures formed by EPCs. For all charts, data represent means ± standard deviations derived from four independent experiments (n = 6). Groups labeled with different lowercase letters are significantly different ($p < 0.05$).

rapamycin (mTOR) were significantly elevated after SCS implantation (Fig. 8A, $p < 0.05$), while the total protein contents of PI3K, Akt, and mTOR were not significantly altered ($p > 0.05$). Compared with control medium, DRG cells cultured with silicon supplemented medium also showed increased phosphorylation level of the PI3K/AKT/mTOR signaling pathway (Fig. 8B, $p < 0.05$). The results suggest that the PI3K/Akt/mTOR signaling pathway is activated in SCS-upregulated bone regeneration.

8. Discussion

Studies of humans and other species have suggested the potential of Si in regulating bone metabolism. Nevertheless, the underlying reason for this favorable effect remains obscure. The present study provides compelling evidence of the ability of SCS to enhance bone regeneration, with elucidation of the underlying mechanism. The beneficial effects of Si appear to be mediated by Sema3A, an axonal guidance molecule released from sensory neurons. A previously unrecognized Sema3A-mediated cross-talk between sensory nerves and bone regeneration has been identified as the major mechanism underlying Si-induced bone formation. In addition, the mTOR signaling pathway has been shown to regulate Sema3A production.

A growing body of evidence supports the physiological role of Si in bone formation. Silicon has been reported to stimulate bone mineralization and collagen synthesis [33]. Silicon supplement demonstrates long-term efficacy and safety in the treatment of osteoporosis [34]. Neoangiogenesis plays an important role in tissue regeneration by providing adequate nutrition. Silicon has also been considered a potent element that promotes angiogenesis at therapeutic doses [35]. Release of silicic acid is considered to be the major factor in promoting

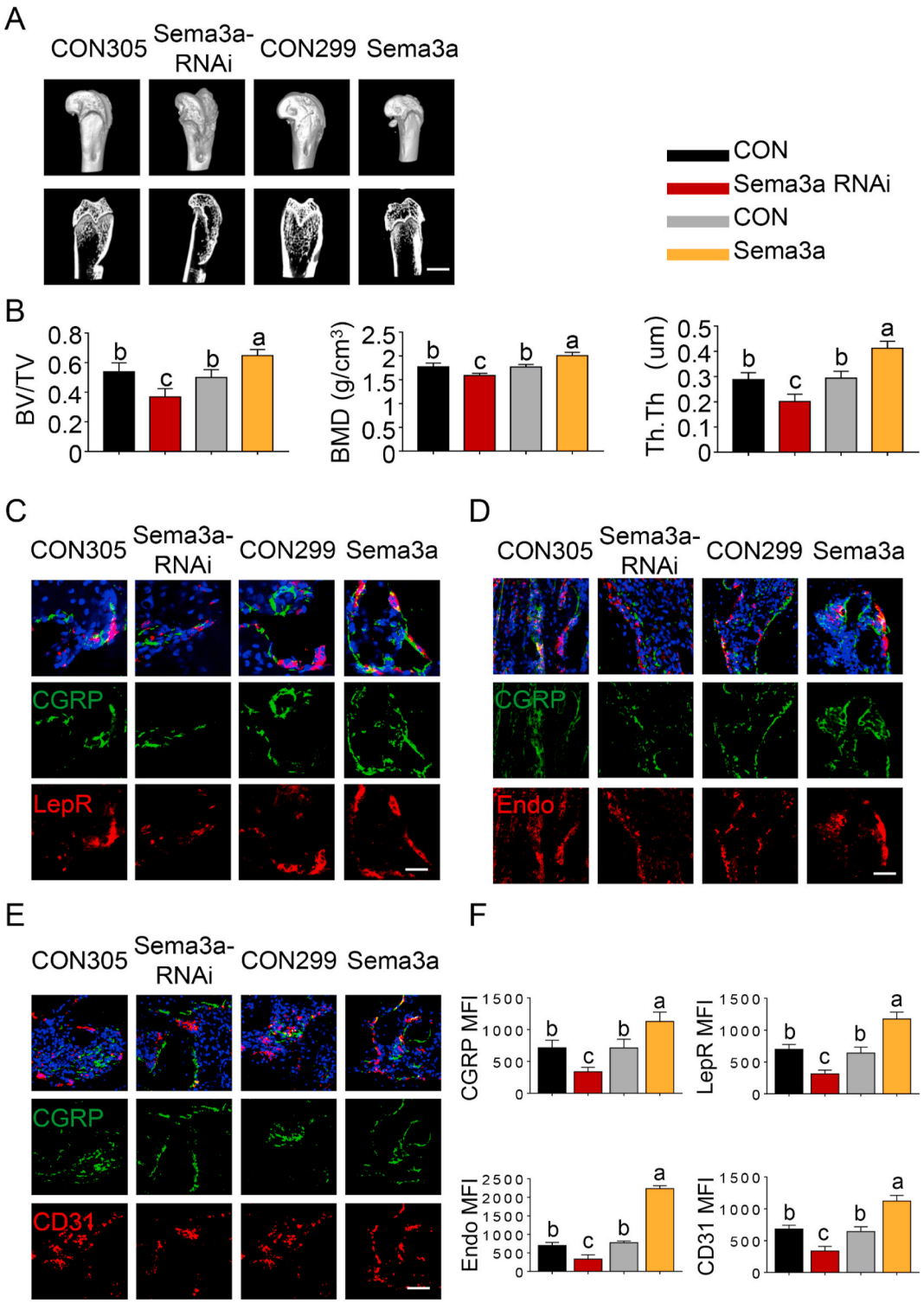

Fig. 7. Sensory nerve-derived Sema3A promotes osteogenesis and angiogenesis in SCS-mediated bone regeneration. (**A**) Micro-CT analysis of bone regeneration at 12 weeks. 3D reconstructed superficial and interior images of femoral condyle defects in different groups. Scale bar: 4 cm. (**B**) Quantitative analysis of bone volume/total volume (TV/BV), bone mineral density (BMD) and Trabecular Thickness (Tb.Th) (n = 6). (**C**) Representative images of immunofluorescence staining of Leptin Receptor and CGRP. (**D**) Representative images of immunofluorescence staining of CGRP and Emcn. (**E**) Representative images of immunofluorescence staining of CGRP and CD31. (**F**) Quantification of CGRP, LepR, Emcn and CD31 median fluorescence intensity (MFI) per field view. Nuclei were stained with DAPI (blue). Scale bar: 100 μm. For all charts, data represent means ± standard deviations (n = 6). Groups labeled with different lowercase letters are significantly different ($p < 0.05$).

osteogenesis of bioceramic materials [36]. Silicic acid molecules that enter cells act as signals for upregulation of genes that generate cell cycle regulator proteins and growth factors [16,37]. In the present study, sensory nerve dysfunction by capsaicin injection or knockdown of Sema3A in DRG resulted in significant inhibition of silicon-induced osteogenesis in the rodent bone defect model. In addition, MSCs and EPCs were activated after they were co-cultured with Si-stimulated DRG. Such findings indicate that the osteogenic potential of SCS is strongly

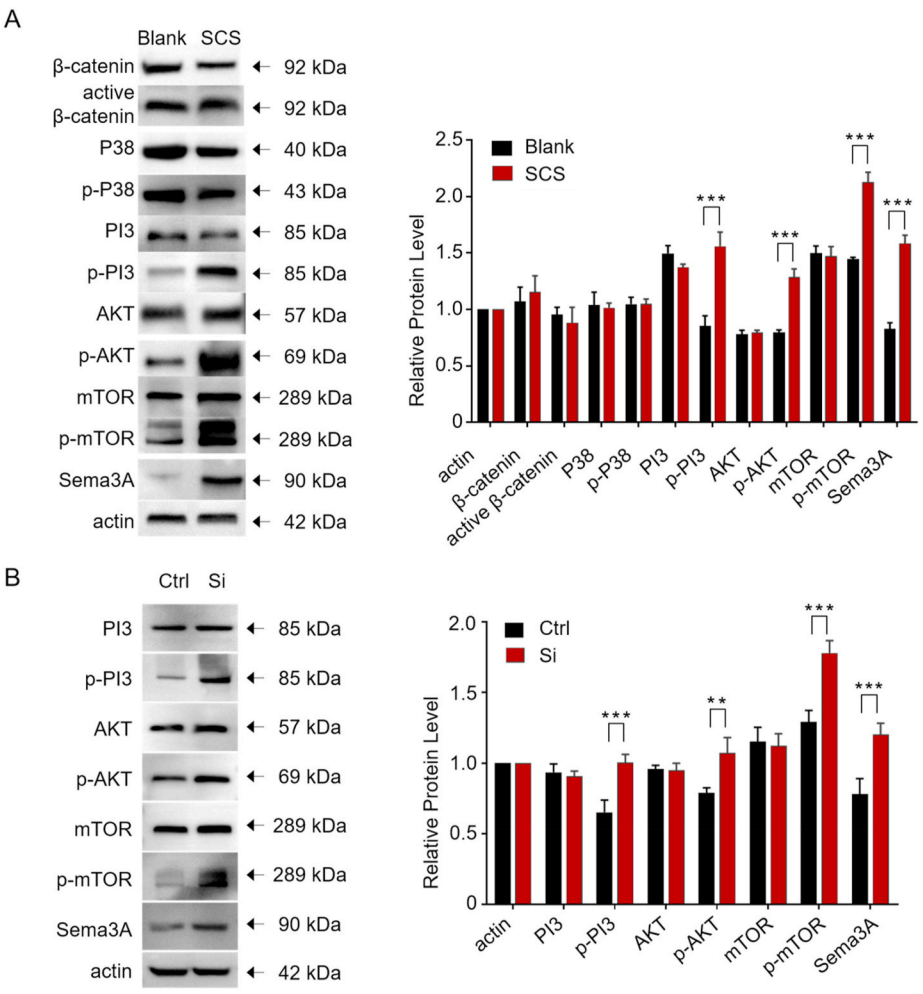

Fig. 8. Activation of the PI3K-Akt-mTOR signaling pathway. (A) DRG tissues obtained from rats with or without SCS implantation and (B) DRG cells cultured with or without silicon-supplemented medium, followed by measurement of protein levels associated with the signaling pathways. Western blot data indicated that Akt-mTOR was activated (**$p < 0.01$, ***$p < 0.001$). Wnt/β-catenin and MAPK/p38 pathways showed no apparent alterations. For all charts, data represent means ± standard deviations ($n = 3$).

dependent on Si functionalization and interaction with sensory nerves.

The outcome of SCS implantation in wound defects *in vivo* is encouraging. The SCSs accelerated bone regeneration, as indicated by the increases in BV/TV, Tb.Th and BMD as well as the extent of *in vivo* calcein staining during the early stage of wound repair. The preponderance of $CGRP^+$ sensory nerves in the SCS group corresponded well with MSC aggregation and increased vessel formation. Chemical cues derived from the SCSs synergistically activated sensory innervation and vascularization. Considering that only a limited number of MSCs, blood vessels and nerve fibers are available in an injury site, immunofluorescence staining and quantification was performed in the present study to analyze the expression profiles of specific proteins and their location. In future studies, it is necessary to verify the present results by evaluating the gene expression of these markers via RT-PCR. Furthermore, single-cell genome sequencing, which is capable of discerning the contributions from distinct cellular populations [38], may be used to separately detect the changes in gene expression of MSCs, blood vessels and nerve fibers. Because there was no increase in pain level in rats that received SCS treatment, it may be surmised that biosilicification helps improve the osteoinductivity of the implanted collagen scaffolds. Additional studies have to be performed on the efficacy of SCSs using more clinically-relevant bone defect models prior to their clinical use for treating bone diseases/injuries such as osteoporotic fracture, diabetic bone metabolism and other traumatic injury. Silicon supplement has been reported to have a good safety profile in the literature [39]. The present results show that there was no significant difference in the plasma levels of inflammatory factors between the SCS-implanted group and the blank control group ($p > 0.05$ for all comparisons) (SI-4). As for effects on pain sensation, there were no significant changes in pain withdrawal responses between the groups of animals receiving blank or SCS implantation ($p > 0.05$ for all comparisons) (SI-5). The *in vitro* effects of soluble Si, existing predominantly as orthosilicic acid, have been investigated extensively within the physiological concentration range (2–30 μM) [40,41]. To the best of our understanding, this is the first time that DRG neurons have been co-cultured with orthosilicate *in vitro*. In the present study, decreased neurite length and DRG cell number were identified in DRGs that were cultured in neurobasal medium supplemented with 40 μM silicon, compared the DRGs that were cultured in control medium. The neurotoxic effect may be attributed to limited pH buffering capacity [42] and sensitive N-methyl-D-aspartate receptor activation [43] in that neurobasal medium that was supplemented with orthosilicate. Further studies are required to clarify the mechanism for the adverse effects of DRGs after their exposure to a high concentration of orthosilicate.

Another high-yielding fruit that arises from the present study is the generation of a silicified biomaterial using a facile strategy. Synthesis of SCS is usually achieved by pretreatment of collagen fibrils with polycationic molecules such as poly(allylamine) hydrochloride. However, poly(allylamine) hydrochloride has dose-dependent toxicity and is not approved as a pharmaceutical ingredient [44]. Although choline supplement has limited value in bone metabolism [45], choline-stabilized soluble silica is believed to have high bioavailability compared with other Si supplements [46]. Accordingly, choline chloride was used in the present work to stabilize the silicifying medium as the first step of intrafibrillar silicification. Liquid chromatography is a common method for quantitative determination of choline chloride [47]. However,

choline chloride in the SCS extract could not be detected by liquid chromatography. This may be due to the low concentration of choline chloride released from the SCS. Further studies are needed to clarify whether choline chloride is released, as well as the biological role of choline in bone health. The SCS possesses a highly-mineralized surface morphology that creates microscale surface roughness to enhance cell attachment. Compared with a native collagen scaffold, the SCS has increased porosity and improved tensile properties. The increased scaffold volume after silicification creates a high degree of porosity. In addition, effective deposition of intrafibrillar silica can enhance the mechanical strength of the collagen matrix. This, in turn, augments the tensile modulus of the silicified collagen matrix. Increased porosity and tensile modulus of the SCS also promote cell infiltration and proliferation and create a scaffold with better mechanical stability [48]. The SCS has the ability to release silicic acid. This, in turn, enhances bone regeneration through peripheral sensory nerves.

Deprivation of Sema3A from sensory neurons disrupts nerve fiber organization and adversely affects skeletal vascularization and mineralization. Both the *in vitro* and *in vivo* results in the present work support that Si upregulates neural Sema3A production to promote osteogenic differentiation. Inhibition of Sema3A expression *in vivo* attenuated new bone formation induced by SCS implantation, whereas overexpression of Sema3A enhanced new bone formation. Bone cells express receptors for Sema3A and activation of those receptors has profound effects on promoting angiogenesis in bone [49]. A previous study reported that Sema3A is a powerful protein that promotes osteogenic differentiation of bone marrow MSCs [50]. Exogenous Sema3A exerts direct control on the rate of migration of endothelial cells and integrin affinity; these factors are indispensable for new blood vessel formation [51]. A drug-delivery system based on Sema3A gene therapy ameliorated bone loss in osteoporotic ovariectomized mice [52]. Sema3A is a selective repellent of SP-positive and CGRP-positive sensory nerve fibers. The ability of Sema3A to inhibit aberrant sensory sprouting suggests that this protein possess neuropathic pain-sparing effects [53]. Although deletion of Sema3A from cells of the osteoblast lineage does not affect sensory innervation or bone volume, mice lacking Sema3A in neurons have decreased sensory innervation of bone and diminished postnatal bone mass [54]. The present RT-PCR and immunofluorescence results showed that Sema3A expression was significantly increased when the DRGs were stimulated by silicate. Moreover, the osteogenic and angiogenic effects of Si-stimulated DRG were blocked by the application of Sema3A neutralizing antibody. Based on previous reports on the osteogenic and angiogenic effects of Sema3A and the present results, we conclude that Si promotes Sema3A secretion from DRGs to enhance the migration, osteogenesis and angiogenesis of MSCs/EPCs.

In the present study, CGRP expression was significantly increased after SCS implantation in the injured site; Sema3A was concomitantly overexpression in the DRGs. These results insinuate that sensory nerves propagate and form functional connections after damage to neighboring axons. Previous research has demonstrated that injury to adult spinal cord induces Sema3A expression and sprouting of CGRP nerve fibers [55]. The amount of Sema3A produced by sensory nerves is low and intraspinal overexpression of Sema3A impedes abnormal innervation [56]. These findings demonstrate that mature sensory afferents maintain their responsiveness to Sema3A in a dose-dependent manner. Although Sema3A may be used therapeutically to control sensory sprouting, the developmental changes in Sema3A and its dynamic relationship with nerve terminal plasticity are not known. In addition, the level of Sema3A increased significantly in femur injury sites after the implantation of SCS, while inhibition of sensory nerve by capsaicin blocked the upregulation in Sema3A expression (SI-9). Because SCS promotes Sema3A expression in DRGs as well as the distribution of CGRP-positive sensory nerves, the increased expression of Sema3A in femur injury sites could have resulted from the increased innervation of sensory nerve after SCS implantation. Thus, Sema3A may be literally perceived as the ambassador of neural-osteogenic interaction.

Simultaneous changes in the levels of Sema3A and p-mTOR *in vivo* suggest that activation of the mTOR pathway is associated with elevated Sema3A level in the SCS group. This relation between mTOR pathway and Sema3A has also been demonstrated in diabetic keratinocytes [57] and in renal tissue with acute kidney injury [58]. New insights on mTOR function have been elucidated over the past several years. In particular, local protein synthesis mediated by mTOR was found to participate in the development of axons and dendrites, as well as in regulating the transmission of pain signals [59]. It is now clear that the mTOR pathway plays a central role in sensing environmental conditions and regulating metabolism at both the cellular and organismal level. The present study provides a unique perspective on the role of Si in regulating the mTOR pathway in the nervous system. Further studies are required to validate the above results by probing the signal transduction process. This may be achieved by using AKT-mTOR inhibitors in *in vitro* Si stimulation of DRG and in *in vivo* bone defect models.

The neglect of the significance vascular and nervous networks in bone regeneration is likely to be an important reason for the delayed or impaired recovery of bone defects. Bone implant materials that can integrate both nerve and vessel regeneration have not been actively pursued by scientists because of the difficulty in regulating multiple tissue types [60]. The SCS investigated in the present study provides a prototype for the development of a neurovascular bone implant material that can reproduce the microenvironment of bone tissue and induce bone healing via promotion of angiogenesis and improved nerve innervation. A more comprehensive understanding of the process of vascularization and neuralization, and their synergistic interactions for promoting osteogenesis is expected.

9. Conclusion

Within the limits of the present study, it may be concluded that the excellent osteoinductivity of SCS is associated with sensory Sema3A production. Silicified collagen scaffolds demonstrate potential for clinical translation by integrating the functions of innervation, vascularization and tissue mineralization into a single scaffold. More importantly, the present study provides preliminary understanding of the sensory nerve mechanism underlying the effects of SCS on *in-situ* bone regeneration.

CRediT authorship contribution statement

Yu-Xuan Ma: Conceptualization, Methodology, Writing – original draft. **Kai Jiao:** Conceptualization, Methodology, Writing – original draft. **Qian-Qian Wan:** Conceptualization, Methodology, Writing – original draft. **Jing Li:** Validation, Formal analysis, Investigation. **Ming-Yi Liu:** Validation, Formal analysis, Investigation. **Zi-Bin Zhang:** Validation, Formal analysis, Investigation. **Wen Qin:** Validation, Formal analysis, Investigation. **Kai-Yan Wang:** Validation, Formal analysis, Investigation. **Ya-zhou Wang:** Resources, Ji-Hua Chen, Resources. **Franklin R. Tay:** Writing – review & editing. **Li-Na Niu:** Supervision, Funding acquisition.

Declaration of competing interest

A patent has been applied for the novel biomimetic silicification process utilizing choline chloride as both the collagen pretreatment agent and silica stabilizer.

Acknowledgments

This work was supported by grants 81722015, 81870805, 81870787, 81671012 and 81720108011 from National Nature Science Foundation of China, grant 2020TD-033 from the Shaanxi Key Scientific and Technological Innovation Team and by the Youth Innovation Team of Shaanxi Universities.

Appendix A. Supplementary data

Supplementary data to this article can be found online at https://doi.org/10.1016/j.bioactmat.2021.07.016.

References

[1] S. Grässel, The role of peripheral nerve fibers and their neurotransmitters in cartilage and bone physiology and pathophysiology, Arthritis Res. Ther. 16 (2014), https://doi.org/10.1186/s13075-014-0485-1.

[2] G. Sisask, C.J. Silfverswärd, A. Bjurholm, O. Nilsson, Ontogeny of sensory and autonomic nerves in the developing mouse skeleton, Auton. Neurosci. Basic Clin. 177 (2013) 237–243, https://doi.org/10.1016/j.autneu.2013.05.005.

[3] R.E. Tomlinson, Z. Li, Q. Zhang, B.C. Goh, Z. Li, D.L.J. Thorek, L. Rajbhandari, T. M. Brushart, L. Minichiello, F. Zhou, A. Venkatesan, T.L. Clemens, NGF-TrkA signaling by sensory nerves coordinates the vascularization and ossification of developing endochondral bone, Cell Rep. 16 (2016) 2723–2735, https://doi.org/10.1016/j.celrep.2016.08.002.

[4] R.E. Tomlinson, Z. Li, Z. Li, L. Minichiello, R.C. Riddle, A. Venkatesan, T. L. Clemens, NGF-TrkA signaling in sensory nerves is required for skeletal adaptation to mechanical loads in mice, Proc. Natl. Acad. Sci. U. S. A 114 (2017) E3632–E3641, https://doi.org/10.1073/pnas.1701054114.

[5] Z. Li, C.A. Meyers, L. Chang, S. Lee, Z. Li, R. Tomlinson, A. Hoke, T.L. Clemens, A. W. James, Fracture repair requires TrkA signaling by skeletal sensory nerves, J. Clin. Invest. 129 (2019) 5137–5150, https://doi.org/10.1172/JCI128428.

[6] Y. Ding, M. Arai, H. Kondo, A. Togari, Effects of capsaicin-induced sensory denervation on bone metabolism in adult rats, Bone 46 (2010) 1591–1596, https://doi.org/10.1016/j.bone.2010.02.022.

[7] S.C. Offley, T.Z. Guo, T. Wei, J.D. Clark, H. Vogel, D.P. Lindsey, C.R. Jacobs, W. Yao, N.E. Lane, W.S. Kingery, Capsaicin-sensitive sensory neurons contribute to the maintenance of trabecular bone integrity, J. Bone Miner. Res. 20 (2005) 257–267, https://doi.org/10.1359/JBMR.041108.

[8] H. He, J. Chai, S. Zhang, L. Ding, P. Yan, W. Du, Z. Yang, CGRP may regulate bone metabolism through stimulating osteoblast differentiation and inhibiting osteoclast formation, Mol. Med. Rep. 13 (2016) 3977–3984, https://doi.org/10.3892/mmr.2016.5023.

[9] T. Niedermair, S. Schirner, R. Seebröker, R.H. Straub, S. Grässel, Substance P modulates bone remodeling properties of murine osteoblasts and osteoclasts, Sci. Rep. 8 (2018) 1–15, https://doi.org/10.1038/s41598-018-27432-y.

[10] L. Verlinden, D. Vanderschueren, A. Verstuyf, Semaphorin signaling in bone, Mol. Cell. Endocrinol. 432 (2016) 66–74, https://doi.org/10.1016/j.mce.2015.09.009.

[11] A. Ibrahim, 3D Bioprinting Bone, Elsevier Ltd., 2018, https://doi.org/10.1016/B978-0-08-101103-4.00015-6.

[12] G. Lalwani, M. D'Agati, B. Farshid, B. Sitharaman, in: Carbon and Inorganic Nanomaterial-Reinforced Polymeric Nanocomposites for Bone Tissue Engineering, Elsevier Ltd, 2016, https://doi.org/10.1016/B978-1-78242-452-9.00002-9.

[13] J.J. Fan, T.W. Mu, J.J. Qin, L. Bi, G.X. Pei, Different effects of implanting sensory nerve or blood vessel on the vascularization, neurotization, and osteogenesis of tissue-engineered bone in vivo, BioMed Res. Int. 2014 (2014), https://doi.org/10.1155/2014/412570.

[14] T. Liang, J. Wu, F. Li, Z. Huang, Y. Pi, G. Miao, W. Ren, T. Liu, Q. Jiang, L. Guo, Drug-loading three-dimensional scaffolds based on hydroxyapatite-sodium alginate for bone regeneration, J. Biomed. Mater. Res. (2020), https://doi.org/10.1002/jbm.a.37018.

[15] Y. Zhang, J. Xu, Y.C. Ruan, M.K. Yu, M. O'Laughlin, H. Wise, D. Chen, L. Tian, D. Shi, J. Wang, S. Chen, J.Q. Feng, D.H.K. Chow, X. Xie, L. Zheng, L. Huang, S. Huang, K. Leung, N. Lu, L. Zhao, H. Li, D. Zhao, X. Guo, K. Chan, F. Witte, H. C. Chan, Y. Zheng, L. Qin, Implant-derived magnesium induces local neuronal production of CGRP to improve bone-fracture healing in rats, Nat. Med. 22 (2016) 1160–1169, https://doi.org/10.1038/nm.4162.

[16] W. Götz, E. Tobiasch, S. Witzleben, M. Schulze, Effects of silicon compounds on biomineralization, osteogenesis, and hard tissue formation, Pharmaceutics 11 (2019) 1–27, https://doi.org/10.3390/pharmaceutics11030117.

[17] X. Zhou, N. Zhang, S. Mankoci, N. Sahai, Silicates in orthopedics and bone tissue engineering materials, J. Biomed. Mater. Res. 105 (2017) 2090–2102, https://doi.org/10.1002/jbm.a.36061.

[18] E. Foglio, B. Buffoli, C. Exley, R. Rezzani, L.F. Rodella, Regular consumption of a silicic acid-rich water prevents aluminium-induced alterations of nitrergic neurons in mouse brain : histochemical and immunohistochemical studies. https://doi.org/10.14670/HH-27.1055, 2015.

[19] D.D. Hunter, V. Castranova, C. Stanley, R.D. Dey, Effects of silica exposure on substance p immunoreactivity and preprotachykinin mrna expression in trigeminal sensory neurons in fischer 344 rats, J. Toxicol. Environ. Health Part A. 53 (1998) 593–605, https://doi.org/10.1080/009841098159051.

[20] J. long Sun, K. Jiao, L. na Niu, Y. Jiao, Q. Song, L. juan Shen, F.R. Tay, J. hua Chen, Intrafibrillar silicified collagen scaffold modulates monocyte to promote cell homing, angiogenesis and bone regeneration, Biomaterials 113 (2017) 203–216, https://doi.org/10.1016/j.biomaterials.2016.10.050.

[21] L.N. Niu, K. Jiao, Y.P. Qi, S. Nikonov, C.K.Y. Yiu, D.D. Arola, S.Q. Gong, A. El-Marakby, M.R.O. Carrilho, M.W. Hamrick, K.M. Hargreaves, A. Diogenes, J. H. Chen, D.H. Pashley, F.R. Tay, Intrafibrillar silicification of collagen scaffolds for sustained release of stem cell homing chemokine in hard tissue regeneration, Faseb. J. 26 (2012) 4517–4529, https://doi.org/10.1096/fj.12-210211.

[22] C.N. Bedbrook, B.E. Deverman, V. Gradinaru, Viral strategies for targeting the central and peripheral nervous systems, Annu. Rev. Neurosci. 41 (2018) 323–348, https://doi.org/10.1146/annurev-neuro-080317-062048.

[23] Y. Zhang, N. Cheng, R. Miron, B. Shi, X. Cheng, Delivery of PDGF-B and BMP-7 by mesoporous bioglass/silk fibrin scaffolds for the repair of osteoporotic defects, Biomaterials 33 (2012) 6698–6708, https://doi.org/10.1016/j.biomaterials.2012.06.021.

[24] J.R. Deuis, L.S. Dvorakova, I. Vetter, Methods used to evaluate pain behaviors in rodents, Front. Mol. Neurosci. 10 (2017) 1–17, https://doi.org/10.3389/fnmol.2017.00284.

[25] J. Guan, J. Zhang, S. Guo, H. Zhu, Z. Zhu, H. Li, Y. Wang, C. Zhang, J. Chang, Human urine-derived stem cells can be induced into osteogenic lineage by silicate bioceramics via activation of the Wnt/β-catenin signaling pathway, Biomaterials 55 (2015) 1–11, https://doi.org/10.1016/j.biomaterials.2015.03.029.

[26] M.Y. Shie, S.J. Ding, Integrin binding and MAPK signal pathways in primary cell responses to surface chemistry of calcium silicate cements, Biomaterials 34 (2013) 6589–6606, https://doi.org/10.1016/j.biomaterials.2013.05.075.

[27] W. Ruolan, C. Liangjiao, S. Longquan, The mTOR/ULK1 signaling pathway mediates the autophagy-promoting and osteogenic effects of dicalcium silicate nanoparticles, J. Nanobiotechnol. 18 (2020) 1–19, https://doi.org/10.1186/s12951-020-00663-w.

[28] S.J. Sample, Z. Hao, A.P. Wilson, P. Muir, Role of Calcitonin gene-related peptide in bone repair after cyclic fatigue loading, PloS One 6 (2011), https://doi.org/10.1371/journal.pone.0020386.

[29] B.O. Zhou, R. Yue, M.M. Murphy, J.G. Peyer, S.J. Morrison, Leptin-receptor-expressing mesenchymal stromal cells represent the main source of bone formed by adult bone marrow, Cell Stem Cell 15 (2014) 154–168, https://doi.org/10.1016/j.stem.2014.06.008.

[30] A.P. Kusumbe, S.K. Ramasamy, R.H. Adams, Coupling of angiogenesis and osteogenesis by a specific vessel subtype in bone, Nature 507 (2014) 323–328, https://doi.org/10.1038/nature13145.

[31] L. Guo, J. Hamre, S. Eldridge, H.P. Behrsing, F.M. Cutuli, J. Mussio, M. Davis, Multiparametric image analysis of rat dorsal root ganglion cultures to evaluate peripheral neuropathy- inducing chemotherapeutics, Toxicol. Sci. 156 (2017) 275–288, https://doi.org/10.1093/toxsci/kfw254.

[32] T. Negishi-Koga, M. Shinohara, N. Komatsu, H. Bito, T. Kodama, R.H. Friedel, H. Takayanagi, Suppression of bone formation by osteoclastic expression of semaphorin 4D, Nat. Med. 17 (2011) 1473–1480, https://doi.org/10.1038/nm.2489.

[33] L.M. Jurkić, I. Cepanec, S.K. Pavelić, K. Pavelić, Biological and therapeutic effects of ortho-silicic acid and some ortho-silicic acid-releasing compounds: new perspectives for therapy, Nutr. Metab. 10 (2013) 1–12, https://doi.org/10.1186/1743-7075-10-2.

[34] G. Schwarz, B. Aa, Cobalt in human health and disease, Met. Ions Life Sci. 13 (2013) 295–320, https://doi.org/10.1007/978-94-007-7500-8.

[35] K. Dashnyam, J.O. Buitrago, T. Bold, N. Mandakhbayar, R.A. Perez, J.C. Knowles, J.H. Lee, H.W. Kim, Angiogenesis-promoted bone repair with silicate-shelled hydrogel fiber scaffolds, Biomater. Sci. 7 (2019) 5221–5231, https://doi.org/10.1039/c9bm01103j.

[36] C.D.S. Ranmuthu, C.K.I. Ranmuthu, J.C. Russell, D. Singhania, W.S. Khan, Evaluating the effect of non-cellular bioactive glass-containing scaffolds on osteogenesis and angiogenesis in in vivo animal bone defect models, Front. Bioeng. Biotechnol. 8 (2020) 1–16, https://doi.org/10.3389/fbioe.2020.00430.

[37] S.J. Wang, D. Jiang, Z.Z. Zhang, Y.R. Chen, Z.D. Yang, J.Y. Zhang, J. Shi, X. Wang, J.K. Yu, Biomimetic nanosilica–collagen scaffolds for in situ bone regeneration: toward a cell-free, one-step surgery, Adv. Mater. 31 (2019) 1–10, https://doi.org/10.1002/adma.201904341.

[38] C. Gawad, W. Koh, S.R. Quake, Single-cell genome sequencing: current state of the science, Nat. Rev. Genet. 17 (2016) 175–188, https://doi.org/10.1038/nrg.2015.16.

[39] L. AL Araújo, F. Addor, P.M. Campos, Use of silicon for skin and hair care: an approach of chemical forms available and efficacy, An. Bras. Dermatol. 91 (2016) 331–335, https://doi.org/10.1590/abd1806-4841.20163986.

[40] M. Xing, X. Wang, E. Wang, L. Gao, J. Chang, Bone tissue engineering strategy based on the synergistic effects of silicon and strontium ions, Acta Biomater. 72 (2018) 381–395, https://doi.org/10.1016/j.actbio.2018.03.051.

[41] D. M Reffitt, N. Ogston, R. Jugdaohsingh, H.F. Cheung, B.A. Evans, R.P. Thompson, J.J. Powell, G.N. Hampson, Orthosilicic acid stimulates collagen type 1 synthesis and osteoblastic differentiation in human osteoblast-like cells in vitro, Bone 32 (2003) 127–135, https://doi.org/10.1016/s8756-3282(02)00950-x.

[42] V. Petrović, V. Opačić-Galić, S. Živković, B. Nikolić, V. Danilović, V. Miletić, V. Jokanović, D. Mitić-Ćulafić, Biocompatibility of new nanostructural materials based on active silicate systems and hydroxyapatite: in vitro and in vivo study, Int. Endod. 48 (2015) 966–975, https://doi.org/10.1111/iej.12391. Epub 2014 Nov 5.

[43] J. Hogins, D.C. Crawford, C.F. Zorumski, S. Mennerick, Excitotoxicity triggered by Neurobasal culture medium, PloS One 6 (2011), e25633, https://doi.org/10.1371/journal.pone.0025633. Epub 2011 Sep. 28.

[44] D. Di Silvio, M. Martínez-Moro, C. Salvador, M. de los Angeles Ramirez, P. R. Caceres-Velez, M.G. Ortore, D. Dupin, P. Andreozzi, S.E. Moya, Self-assembly of poly(allylamine)/siRNA nanoparticles, their intracellular fate and siRNA delivery, J. Colloid Interface Sci. 557 (2019) 757–766, https://doi.org/10.1016/j.jcis.2019.09.082.

[45] A.A. Gorustovich, A.A. Espósito, M.B. Guglielmotti, M.J. Giglio, Mandibular bone remodeling under a choline-deficient diet: a histomorphometric study in rats, J. Periodontol. 74 (2003) 831–837, https://doi.org/10.1902/jop.2003.74.6.831.

[46] A. Barel, M. Calomme, A. Timchenko, K. De Paepe, N. Demeester, V. Rogiers, P. Clarys, D. Vanden Berghe, Effect of oral intake of choline-stabilized orthosilicic acid on skin, nails and hair in women with photodamaged skin, Arch. Dermatol. Res. 297 (2005) 147–153, https://doi.org/10.1007/s00403-005-0584-6.
[47] M.M. Phillips, Analytical approaches to determination of total choline in foods and dietary supplements, Anal. Bioanal. Chem. 403 (2012) 2103–2112, https://doi.org/10.1007/s00216-011-5652-5.
[48] J. Will, R. Detsch, A.R. Boccaccini, in: Structural and Biological Characterization of Scaffolds, Elsevier, 2013, https://doi.org/10.1016/B978-0-12-415800-9.00008-5.
[49] M. Hayashi, T. Nakashima, M. Taniguchi, T. Kodama, A. Kumanogoh, H. Takayanagi, Osteoprotection by semaphorin 3A, Nature 485 (2012) 69–74, https://doi.org/10.1038/nature11000.
[50] Q. Qiao, X. Xu, Y. Song, S. Song, W. Zhu, F. Li, Semaphorin 3A promotes osteogenic differentiation of BMSC from type 2 diabetes mellitus rats, J. Mol. Histol. 49 (2018) 369–376, https://doi.org/10.1007/s10735-018-9776-1.
[51] G. Serini, D. Valdembri, S. Zanivan, G. Morterra, C. Burkhardt, F. Caccavari, L. Zammataro, L. Primo, L. Tamagnone, M. Logan, M. Tessier-Lavigne, M. Taniguchi, A.W. Püschel, F. Bussolino, Class 3 semaphorins control vascular morphogenesis by inhibiting integrin function, Nature 424 (2003) 391–397, https://doi.org/10.1038/nature01784.
[52] K. Yang, R.J. Miron, Z. Bian, Y.F. Zhang, A bone-targeting drug-delivery system based on Semaphorin 3A gene therapy ameliorates bone loss in osteoporotic ovariectomized mice, Bone 114 (2018) 40–49, https://doi.org/10.1016/j.bone.2018.06.003.
[53] M. Hayashi, Y. Kamiya, H. Itoh, T. Higashi, T. Miyazaki, K. Funakoshi, N. Yamashita, Y. Goshima, T. Andoh, Y. Yamada, T. Goto, Intrathecally administered Sema3A protein attenuates neuropathic pain behavior in rats with chronic constriction injury of the sciatic nerve, Neurosci. Res. 69 (2011) 17–24, https://doi.org/10.1016/j.neures.2010.09.006.
[54] T. Fukuda, S. Takeda, R. Xu, H. Ochi, S. Sunamura, T. Sato, S. Shibata, Y. Yoshida, Z. Gu, A. Kimura, C. Ma, C. Xu, W. Bando, K. Fujita, K. Shinomiya, T. Hirai, Y. Asou, M. Enomoto, H. Okano, A. Okawa, H. Itoh, Sema3A regulates bone-mass accrual through sensory innervations, Nature 497 (2013) 490–493, https://doi.org/10.1038/nature12115.
[55] A.A. Cameron, G.M. Smith, D.C. Randall, D.R. Brown, A.G. Rabchevsky, Genetic manipulation of intraspinal plasticity after spinal cord injury alters the severity of autonomic dysreflexia, J. Neurosci. 26 (2006) 2923–2932, https://doi.org/10.1523/JNEUROSCI.4390-05.2006.
[56] X.Q. Tang Xq, D.L. Tanelian, G.M. Smith, Semaphorin3A inhibits nerve growth factor-induced sprouting of nociceptive afferents in adult rat spinal cord, J. Neurosci. 24 (2004) 819–827, https://doi.org/10.1523/JNEUROSCI.1263-03.2004.
[57] L. yan Wu, M. Li, M.L. Qu, X. Li, L.H. Pi, Z. Chen, S.L. Zhou, X.Q. Yi, X.J. Shi, J. Wu, S. Wang, High glucose up-regulates Semaphorin 3A expression via the mTOR signaling pathway in keratinocytes: a potential mechanism and therapeutic target for diabetic small fiber neuropathy, Mol. Cell. Endocrinol. 472 (2018) 107–116, https://doi.org/10.1016/j.mce.2017.11.025.
[58] M. fang Song, Y. Yang, Z. wei Yi, Z. qi Zhang, X. dong Shen, G. hua Hu, Y. fei Zhu, Sema 3A as a biomarker of the activated mTOR pathway during hexavalent chromium-induced acute kidney injury, Toxicol. Lett. 299 (2018) 226–235, https://doi.org/10.1016/j.toxlet.2018.09.005.
[59] R.A. Saxton, D.M. Sabatini, mTOR signaling in growth, metabolism, and disease, Cell 168 (2017) 960–976, https://doi.org/10.1016/j.cell.2017.02.004.
[60] A. Marrella, T.Y. Lee, D.H. Lee, S. Karuthedom, D. Syla, A. Chawla, A. Khademhosseini, H.L. Jang, Engineering vascularized and innervated bone biomaterials for improved skeletal tissue regeneration, Mater. Today 21 (2018) 362–376, https://doi.org/10.1016/j.mattod.2017.10.005.